The standing toroidal mode oscillations in the magnetosphere-ionosphere system(Dissertation_全文)

AUTHOR(S):

Nakata, Hiroyuki

主論文1

The standing toroidal mode oscillations in the magnetosphere - ionosphere system

Hiroyuki Nakata

Department of Geophysics,
Graduate School of Science,
Kyoto University.

December, 1999.

Abstract

Behaviors of the standing Alfvén oscillation (toroidal mode oscillation) in the magnetosphere-ionosphere coupled system is investigated by using a trapezoid-shape magnetosphere model. In this model, the ionosphere is anisotropic thin conductor and inclined to the main magnetic field. The Alfvén speed is spatially non-uniform and variable. It is obtained that the magnetic perturbation is transmitted across the ionosphere differently in the two cases where the ionospheric electric field perturbation is static (the Pedersen conductivity $>$ the Hall conductivity) and where it is inductive (the Pedersen conductivity $<$ the Hall conductivity). It is notable that the ionospheric Hall current in the inductive condition shields the magnetic field perturbation. This shield effect becomes reduced only in the static condition when the magnetic inclination to the ionosphere becomes smaller because the Pedersen conductivity becomes effectively smaller. When the Alfvén speed in the ionosphere is larger, this shield effect also become reduced only in the inductive condition. The north-south asymmetry of the conjugate ground magnetic perturbations is calculated by using the present model with the ionospheric and magnetospheric parameters based on the IGRF and IRI. It is revealed that the ionospheric electric field is almost static for the fundamental mode oscillation, whereas inductive for the higher harmonic ones. It is also found that the north-south asymmetry of the ground magnetic perturbations depends on not only the L-value but also the magnetic longitude; this is because the ionosphere and magnetic field conditions are not uniform along the longitude. The present calculations qualitatively explain the observational results of 210° Magnetic Meridian chain and Syowa-Iceland conjugate stations.

Contents

1 Introduction **1**

1.1 Geomagnetic pulsations and MHD waves 1

1.2 Interaction of the MHD waves with the ionosphere 5

1.2.1 The MHD wave and the ionospheric Pedersen conductivity 5

1.2.2 Ground magnetic perturbations and the ionospheric current 7

1.2.3 The MHD wave and the anisotropic conducting ionosphere 8

1.3 The compendium of this thesis 11

2 Model and Basic Equations **13**

2.1 Model 13

2.2 Basic equation and ionospheric boundary conditions 14

3 Fundamental Character of the standing Alfvén oscillation in the magnetosphere-ionosphere coupled system **17**

3.1 North-south symmetric case 19

3.1.1 Ionospheric conductivity 19

3.1.2 Magnetic inclination 22

3.1.3 Equator-ionosphere V_A ratio 23

3.2 North-south asymmetric case 25

3.2.1 Ionospheric conductivity 26

3.2.2 Magnetic inclination 28

3.2.3 Equator-ionosphere V_A ratio 28

3.3 The latitudinal wave number and the height of the ionosphere 30

4 North-south asymmetry of the ground magnetic perturbations in the realistic model 32

4.1 Assignment of the realistic physical values 33

4.2 Characteristic features of asymmetry of the conjugate ground magnetic perturbations 35

4.3 Comparison with observations 37

4.3.1 Comparison with the observation of 210° magnetic meridian chain . 37

4.3.2 Comparison with the observation of Syowa-Iceland conjugate stations 39

5 Conclusion and Summary 41

A Transmission of the Alfvén Wave through the Ionosphere 45

Chapter 1

Introduction

1.1 Geomagnetic pulsations and MHD waves

Geomagnetic pulsations are the ultra-low-frequency (ULF) perturbations of the ground magnetic field with periods ranging from seconds to minutes. The geomagnetic pulsations are categorized into two groups. One of them is called as the Pc pulsation that shows the continuously sinusoidal variations. Thus the Pc pulsation has a sharp spectral peak and its frequency is almost constant. The other is the Pi pulsation that exhibits rather irregular variation. The Pi pulsation has broad spectral peaks compared with those of the Pc pulsation. The Pc and Pi pulsations were first categorized into five and two groups, respectively, according to their frequencies [Jacob *et al.*, 1964]. At the present time, including new groups, the Pc and Pi pulsations are classified into six and three groups as shown in Figure 1.1 [Saito, 1978].

Several generation mechanisms of the pulsations have been presented. For example, it is widely accepted that the Pi 2 pulsation is closely related to the onset of the substorm. Yumoto [1990] suggested that the Pi 2 pulsation is excited by the cavity mode oscillation [Kivelson *et al.*, 1984; Allan *et al.*, 1986] due to the magnetic field dipolarization or the current disruption suggested by McPherron *et al.* [1973] [c.f. Figure 1.2] The current disruption is equivalent to the eastward current which cancel the cross-tail current. Col-

lapse of the cross-tail current triggers the field aligned current (FAC) flowing into and out of the ionosphere and the ionospheric current connecting the pair of FAC. This current system is called the substorm current wedge [Clauer and McPherron, 1974; Samson, 1982]. The fast magnetosonic mode wave emitted at the current disruption event induces the cavity mode oscillation. This scenario is believed to be the generation mechanism of the Pi 2 pulsation. Thus, the Pi 2 pulsation is mainly observed in the night-side in the magnetosphere as shown in Figure 1.3 [Takahashi *et al.*, 1992].

The Pc pulsations are mainly observed in the day-side. The compressional Pc 3 pulsation is closely related to the upstream wave in the magnetosheath [Scarf *et al.*, 1970], which penetrates the magnetosphere [Zhang *et al.*, 1993]. Furthermore, the interplanetary shock also induces the toroidal mode Pc 3-4 pulsations [Yumoto *et al.*, 1994]. The Pc 3 pulsation is observed on the ground as the daytime Pc pulsation with long duration. The long duration of the pulsation suggests the oscillation standing along a magnetic field line between the ionospheres in the northern and southern hemispheres. The standing oscillation along the field line is the Alfvén mode oscillation as explained later. The toroidal Pc 5 pulsation occurs with or without the shorter-period Pc 3-4 pulsation. Nosé *et al.* [1995] shows that the Pc 5 pulsation is mainly observed in the high latitude [c.f. Figure 1.4]. The Pc 5 pulsation in high latitudes may be the fundamental mode of the standing Alfvén oscillation and that the Pc 3-4 pulsations are higher harmonics of the standing Alfvén oscillation. The Kelvin-Helmholtz instability in the magnetopause [Fujita *et al.*, 1996] is also regarded to excite the standing Alfvén oscillations via the field-line resonance [Tamao, 1965; Southwood, 1974; Chen and Hasegawa, 1974] as explained later. Therefore, the standing Alfvén oscillation is regarded to be observed as the Pc pulsation. In the present thesis, we deal with the standing Alfvén oscillation.

As these pulsations transport informations of the magnetosphere, it is very important to know their propagation mechanisms in the standpoint of the magnetospheric physics. In order to study the geomagnetic pulsations, we should know the magnetohydrodynamics (MHD). Since MHD integrates the fluid dynamics and the electro-magnetics, the MHD

waves include the characteristics of the sound wave and the electromagnetic wave. There are compressional and transverse waves in the cold plasma ("cold" means $\beta \ll 1$ where β is defined by the ratio of the plasma pressure to the magnetic pressure). The transverse wave is called the shear Alfvén wave (simply the Alfvén wave or Alfvén mode wave) and transports energy only along the magnetic field line with Alfvén speed (V_A). V_A is defined as

$$V_A = \frac{B_0}{\sqrt{\mu_0 \rho}}, \tag{1.1}$$

where B_0 is the magnitude of the main magnetic field, μ_0 is magnetic permeability in vacuum and ρ is plasma density. The compressional wave, on the contrary, propagates to any direction. If the wave propagates in a warm plasma with finite β, the velocity of the compressional wave is larger than the Alfvén speed. Thus, the compressional waves are also referred to as the fast magnetosonic mode wave (simply the fast mode wave).

Since the Alfvén wave propagates only along the field line, this wave forms a standing oscillation. The geomagnetic pulsation with long duration is the standing MHD oscillation of the magnetic field line. This is due to the Alfvén waves (refer to as a standing Alfvén oscillation). The observational fact that the frequency of the pulsation becomes smaller in the lower latitude reveals existence of the standing oscillation.

As explained above, the Pc pulsation is generated out of the magnetosphere. Therefore, the perturbation has to propagate across the field line to be observed as the geomagnetic pulsations at middle and low latitudes. This fact indicates that the wave first generated is the fast mode wave. Then, how the standing Alfvén wave is induced? The answer is the field-line resonance (FLR) theory. FLR is firstly studied by Tamao [1965] and developed by Southwood [1974] and Chen and Hasegawa [1974]. The scenario of this theory is as follows: the fast mode wave excited out of the magnetosphere, due to the Kelvin-Helmholtz instability or the interplanetary shocks, propagates into the magnetosphere across the field line. When the magnetosphere is nonuniform and the fast mode wave is azimuthally asymmetric, the fast mode wave and the Alfvén mode wave always couple. The fast mode wave resonate with the Alfvén wave on the field line where the frequency of

the fast mode wave becomes the same as the eigenfrequency of the field line (the frequency of the standing Alfvén oscillation). Finally, the standing Alfvén oscillation is excited to be observed as the ground magnetic perturbations.

Before reviewing the interaction between the ionosphere and the MHD waves, we describe physical properties of the MHD waves. Since the MHD approximation requires no electric field parallel to the main magnetic field, general expressions of the electric field of MHD waves can be given as follows.

$$\delta \boldsymbol{E}_\perp = -\nabla_\perp \Phi - \frac{\partial \boldsymbol{A}_\perp}{\partial t}, \tag{1.2}$$

and $\boldsymbol{A} = \nabla \times (\Psi \hat{e})$ where Φ and Ψ are scalar functions and $\hat{e}$ is unit vector along the main magnetic field. As the shear Alfvén wave is irrotational ($\nabla \times \delta \boldsymbol{E} = 0$) and the fast mode wave is source free ($\nabla \cdot \delta \boldsymbol{E} = 0$), the electric field of the Alfvén wave is given by

$$\delta \boldsymbol{E}_\perp = -\nabla_\perp \Phi, \tag{1.3}$$

and that of the fast mode wave is

$$\delta \boldsymbol{E}_\perp = -\frac{\partial}{\partial t} \nabla_\perp \times (\Psi \hat{e}). \tag{1.4}$$

These equations show that the Alfvén wave has the static (or divergent) electric field and the fast mode wave has the inductive (or rotational) one. Bearing in mind that the MHD waves carry the polarization current ($\propto (\omega / V_A)^2 \delta \boldsymbol{E}_\perp$ where ω is the angular frequency of the wave), the Alfvén wave has divergent current and the fast mode wave has rotational current.

1.2 Interaction of the MHD waves with the ionosphere

1.2.1 The MHD wave and the ionospheric Pedersen conductivity

There is the ionosphere between the magnetosphere and the ground. Therefore, the MHD waves in the magnetosphere are modified by the ionosphere and transmitted toward the ground. In order to study the ground magnetic perturbation, we need to consider the ionospheric modification. Namely, the standing Alfvén oscillation should be studied in the magnetosphere-ionosphere coupled system.

First, let us overview incidence of the Alfvén wave on the ionosphere. Many authors have investigated ionospheric modification of the MHD waves. When the Alfvén wave impinges on the ionosphere, the reflection wave is emitted by the Pedersen current [c.f. Scholar, 1970; Maltsev *et al.*, 1977; Mallinckrodt and Carlson, 1978]. Scholer[1970] investigated propagation of the Alfvén wave excited by the sudden disturbance in the magnetic equator. He derived the reflection coefficient of the incident Alfvén wave as follows

$$R = \frac{\Sigma_A - \Sigma_P}{\Sigma_A + \Sigma_P}, \tag{1.5}$$

where Σ_P is the height-integrated Pedersen conductivity and Σ_A is the Alfvén conductance defined as $1/\mu_0 V_A$ [Maltsev *et al.*, 1977; Mallinckrodt and Carlson, 1978]. Using this equation, we calculate the total electric field in the ionosphere in the case of the Alfvén wave incidence;

$$E_{total} = E_{in} + E_{ref} = E_{in}(1 + R). \tag{1.6}$$

Here E_{total} is the total electric field in the ionosphere, E_{in} is the incident electric field and E_{ref} is the reflected electric field. When Σ_P is much larger than Σ_A (this is a daytime condition), $R \simeq -1$ and thus the ionospheric electric field nearly becomes zero. When we consider the Alfvén wave that forms a standing oscillation, the electric field has a

node in the ionosphere and the magnetic field line is anchored on the ionosphere. While the magnetic field perturbation of the standing Alfvén oscillation has an anti-node in the ionosphere. When Σ_P is much smaller than Σ_A (a night-side condition), on the other hand, $R \simeq 1$ and the total ionospheric electric field is twice the input electric field. The electric and magnetic fields of the standing Alfvén oscillation have an anti-node and a node in the ionosphere, respectively.

The ionospheric reflection of the Alfvén wave explained above tells us behavior of the standing Alfvén oscillation. Newton *et al.* [1978] noticed that the harmonic number increases by one when the Pedersen conductivity changes continuously from zero to infinity [c.f. Figure 1.5]. The second harmonic mode for zero Pedersen conductivity with the anti-node of the electric field in the ionosphere becomes the third harmonic mode of the standing Alfvén oscillation with the node in the ionosphere for infinite Pedersen conductivity.

The damping of the standing Alfvén oscillation is also dependent on the Pedersen conductivity. Newton *et al.* [1978] numerically showed that the damping of the standing Alfvén oscillation is maximized for a certain value of Σ_P. Allan and Knox [1979a] studied the toroidal mode oscillation (the standing Alfvén oscillation) and derived its damping coefficient. Then Allan and Knox [1979b] shows that the damping coefficient is proportional to Σ_P for smaller Σ_P and inversely proportional to Σ_P for larger Σ_P. The damping of the standing Alfvén oscillation is caused by the Joule loss in the ionosphere. Here, we explain the damping. When the Pedersen conductivity is quite large, the ionospheric electric field becomes almost zero as shown in Eq.(1.6). Thus the Joule loss($\delta \boldsymbol{J} \cdot \delta \boldsymbol{E}$) caused by the conductivity is vanished. No Pedersen conductivity invokes no ionospheric current and no Joule loss. When the Pedersen conductivity is a finite value, the Joule

loss is derived as follows:

$$\begin{aligned}
\delta \boldsymbol{J} \cdot \delta \boldsymbol{E} &= \Sigma_P \delta \boldsymbol{E}_{total} \cdot \delta \boldsymbol{E}_{total} \\
&= \Sigma_P (1+R)^2 \delta \boldsymbol{E}_{in}^2 \\
&= \Sigma_P \left(\frac{2\Sigma_A}{\Sigma_A + \Sigma_P} \right)^2 \delta \boldsymbol{E}_{in}^2 \\
&= \frac{4\Sigma_P \Sigma_A^2}{(\Sigma_A + \Sigma_P)^2} \delta \boldsymbol{E}_{in}^2 \qquad (1.7)
\end{aligned}$$

From this relation, the Joule loss is maximum when $\Sigma_A = \Sigma_P$ [c.f. Figure 1.6]. We understand that the Alfvén conductance is an important factor for the damping.

1.2.2 Ground magnetic perturbations and the ionospheric current

As the ionosphere is an anisotropic conductor, the ionospheric current flows toward not only the direction of the applied electric field (Pedersen current) but also perpendicular to the applied electric field and the main magnetic field (Hall current).

As thickness of the ionosphere is much smaller than the ionospheric skin depth of the MHD waves with ULF-range frequencies, we regard the ionosphere as a thin sheet. Thus the equations of the ionospheric boundary condition are [Tamao, 1984];

$$\hat{N} \times (\delta \boldsymbol{E}_{\perp,mag} - \delta \boldsymbol{E}_{atm}) = 0, \qquad (1.8)$$

$$\hat{N} \times (\delta \boldsymbol{B}_{mag} - \delta \boldsymbol{B}_{atm}) = \mu_0 \delta \boldsymbol{J}, \qquad (1.9)$$

$$\hat{N} \times (\Sigma_P \delta \boldsymbol{E} \times \hat{N}) + (sn) \Sigma_H \delta \boldsymbol{E} \times \hat{N} = \delta \boldsymbol{J}. \qquad (1.10)$$

Σ_H is the height-integrated conductivity and the suffix "$_{mag}$" means "magnetospheric side of the ionosphere" and "$_{atm}$"means "atmospheric side of the ionosphere". $\delta \boldsymbol{J}$ is the ionospheric current associated with the MHD oscillation. $\hat{N}$ is a unit vector vertical to the ionosphere directing toward the magnetosphere, and sn is 1 in the north ionosphere and -1 in the south ionosphere.

When the Alfvén wave with the static electric field impinges on the ionosphere, the Pedersen current is also associated with the static electric field as shown in Eq.(1.10).

When the magnetic field is vertical to the ionosphere, this Pedersen current closes FAC [Tamao, 1965], and it did not affect the ground magnetic perturbation [Fukushima, 1969] [c.f. Figure 1.7(a)]. However, the Hall current is associated with the inductive electric field. This current produces ground magnetic perturbation [e.g. Nishida, 1964, 1978; Inoue and Horowitz, 1966a,b; Hughes and Southwood, 1976a,b; Poulter and Allan, 1985; McHenry and Clauer, 1987; Allan, 1995] because only the source-free current associated with the inductive electric field in the ionosphere becomes the source of the poloidal ground magnetic perturbation [Figure 1.7(b)]. Full wave solutions of the ground magnetic perturbations shows that the polarization of the Alfvén wave rotates 90°[Nishida, 1964; Hughes and Southwood, 1976a,b].

1.2.3 The MHD wave and the anisotropic conducting ionosphere

When the Alfvén wave is injected to the ionosphere, the reflected Alfvén wave is generated through the ionospheric Pedersen current. Both waves have the static electric field. The Hall current induces the reflected fast mode wave with the inductive electric field. This situation is expressed with mathematical formula derived from Eqs(1.8)∼(1.10) as follows:

$$\nabla \cdot \delta \boldsymbol{J}_\perp - \Sigma_P \nabla \cdot \delta \boldsymbol{E}_\perp = -\Sigma_H \hat{e} \nabla \times \delta \boldsymbol{E}_\perp, \tag{1.11}$$

$$\hat{e} \nabla \times \delta \boldsymbol{J}_\perp - \Sigma_P \hat{e} \nabla \times \delta \boldsymbol{E}_\perp = \Sigma_H \nabla \cdot \delta \boldsymbol{E}_\perp. \tag{1.12}$$

We assume the uniform ionosphere and the magnetic field vertical to the ionosphere in the north hemisphere, $\hat{N} = -\hat{e}$. Eq. (1.11) indicates that "the space charge" and FAC associated with the incident and reflected Alfvén waves (l.h.s) has to correspond to rotation of the inductive electric field (r.h.s.). At the same time, rotation of the inductive electric field (proportional to the compressional magnetic field perturbation) and the associated eddy current (l.h.s. of Eq. (1.12)) of the reflected fast mode wave correspond to divergence of the static electric field (r.h.s.). In the case of the Alfvén wave incidence, nonzero Σ_H induces nonzero r.h.s. of Eq. (1.12). Therefore, Eq. (1.12) demonstrates that the static electric field is always accompanied with the inductive one when the ionosphere

has the Hall conductivity. This means that r.h.s. of Eq. (1.11) remains nonzero. Namely, Eq. (1.11) indicates that the inductive electric field modifies the reflection of the incident Alfvén wave. Finally, we conclude that the ionospheric modification of the Alfvén wave should be treated by considering both ionospheric static and inductive electric fields.

The above discussion indicates that both Pedersen and Hall conductivities modify the ionospheric electric field perturbation and consequently control the ground magnetic field perturbation. In spite of this, the past studies did not treat self-consistently the effect of the inductive electric field to the ground magnetic field perturbation. For example, Poulter and Allan [1985] and Allan [1995] investigated the ground magnetic perturbation associated with the standing Alfvén oscillation. They calculated the ground magnetic perturbations with the following procedure; first, the electric field of the Alfvén wave at the ionosphere with only Σ_P is obtained; next, the Hall current is derived as the product of the ionospheric electric field thus obtained and the Hall conductivity. Then this Hall current produces the ground magnetic perturbation. This procedure is not self-consistent because only Σ_P is taken into account in the first step. The reason why they neglected the inductive electric field is that the inductive field seems not to affect the static field associated with incident Alfvén wave. Of course, difficulty in self-consistent treatment of the ionospheric boundary condition forced them to use such simplified way.

By now, there are few works that treat self-consistently the ionospheric boundary condition for the standing Alfvén oscillation. Previous works devoted themselves to study interaction between the anisotropically conducting ionosphere and the Alfvén wave incident to it. For example, Tamao [1984] calculated the ground magnetic perturbation associated with the Alfvén wave incident to the ionosphere [Figure 1.8]. He showed that the two-step procedure is not valid with the Hall conductivity is large. Namely, the ground magnetic perturbation is not proportional to the Hall conductivity when the Hall conductivity is large. This fact is not reproduced by the two-step procedure adopted by Allan [1995]. Fujita [1985] also showed that the ground magnetic perturbation decreases with the Hall conductivity when the Hall conductivity is large [Figure 1.9]. Recently,

Yoshikawa and Itonaga [1996] examined self-consistently the effect of the inductive electric field in the case of the Alfvén wave incidence. They obtained the reflection coefficient of the Alfvén wave as follows:

$$R = \frac{(\Sigma_A - \Sigma_P)(\Sigma_F - \Sigma_P + \Sigma_{atm}\coth(k_\perp d)) + \Sigma_H^2}{(\Sigma_A + \Sigma_P)(\Sigma_F - \Sigma_P + \Sigma_{atm}\coth(k_\perp d)) - \Sigma_H^2} \tag{1.13}$$

where

$$\Sigma_{atm} = \sqrt{\left(\frac{\omega}{c}\right)^2 - k_\perp^2}, \tag{1.14}$$

$$\Sigma_F = \frac{1}{\mu_0\omega}\sqrt{\left(\frac{\omega}{V_A}\right)^2 - k_\perp^2}, \tag{1.15}$$

ω is the angular frequency, $k_\perp$ is the wave number perpendicular to the main magnetic field, and d is the height of the ionosphere. From this reflection coefficient, they revealed that the inductive electric field is effective to the reflection of the Alfvén wave in the cases of larger Hall conductivity or the higher frequency or the smaller horizontal wave number.

Buchert and Budnik [1997] investigated interaction between the incident Alfvén wave and the ionosphere with the self-consistent procedure. They reported that the ionospheric Hall current strongly modifies the behavior of the Alfvén wave when the wave frequency becomes higher or Σ_H/Σ_P is larger. They also explained the amplification of the electric field by the Lenz's law. The ionospheric electric field associated with the incident Alfvén wave accompanies the Hall current. When the current is temporally increasing, the inductive electric field opposite to the Hall current is induced through the Lenz's law. This inductive field also excited the Hall current, which amplify the incident electric field. Namely, when the inductive electric field is significant, the smaller electric field can close the FAC and the electric field in the ionosphere become small.

Here, let us explain the interaction between the Alfvén wave and the ionosphere with Figure 1.7. When the electric field associated with the Alfvén wave is applied on the ionosphere, FAC is closed via the Pedersen current. The magnetic perturbation of Alfvén wave is enclosed by FAC and the ionospheric Pedersen current [Figure 1.7]. Thus, the ground

magnetic perturbation is not produced by the Pedersen current. Besides, the Hall current produces the magnetic perturbations above and below the ionosphere [Figure 1.7(b)]. Poulter and Allan [1985] and Allan [1985] assumed that the ionospheric electric field is produced by the first process and that the ground magnetic perturbation is produced by the second process. The Lenz's law tells that the rotational electric field is induced when the magnetic perturbation is temporally varied [Figure 1.7(c)]. Note that the electric field perturbation is clockwise when the primary electric field in temporally increasing and the main magnetic field is downward. This secondary electric field again induces the Pedersen current and Hall current. The Pedersen current produces the magnetic perturbations above and below the ionosphere. At last, the Hall current caused by the induced current is linked with FAC [Figure 1.7(d)]. This means that balance of the current system of FAC and the ionospheric current should be varied. When the secondary electric field is not effective, reflection of the Alfvén wave by the ionosphere is decided by the relation of the Alfvén conductance and the Pedersen conductivity. When the secondary electric field is large enough, reflection of the Alfvén wave is strongly controlled by the Hall conductivity. Buchert and Budnik [1997] derived the reflection coefficient of the Alfvén wave including the effect of the Hall conductivity in case of the induction dominated limit and showed as follows:

$$R = \frac{\Sigma_A^2 - \Sigma_P^2 - \Sigma_H^2}{(\Sigma_A + \Sigma_P)^2 + \Sigma_H^2}. \tag{1.16}$$

Off course, this equation is consistent with Eq.(1.13) for inductive limited case ($\omega \to \infty$).

1.3 The compendium of this thesis

In the present thesis, to evaluate the ground magnetic perturbation under the anisotropically conducting ionosphere, we calculate self-consistently electromagnetic perturbations associated with the standing Alfvén oscillation in the magnetosphere - ionosphere coupled system. Moreover, the ionosphere and the magnetosphere are usually regarded to be asymmetric along a magnetic field line with respect to the equator. Then, it is likely that

this asymmetry of the magnetosphere-ionosphere system yields the asymmetry between the conjugate ground magnetic perturbations. It is interesting to predict theoretically the asymmetry. Such calculation is also quite informative to the conjugate ground magnetic observation. Note that this theoretical calculation has not been done yet. Therefore, it is another target of the present thesis to evaluate the north-south asymmetry of the ground magnetic perturbations based on a model calculation.

The structure of the present thesis is as follows. In Chapter 2, we explain the model magnetosphere including the ionosphere and the basic equations used in the present thesis. In Chapter 3, by using the numerical results, we show how the behavior of the standing Alfvén oscillation is controlled by the three parameters, i.e. the ionospheric conductivity, the inclination of the main magnetic field, and the magnetospheric field-aligned Alfvén speed profile. Ionospheric transmission of the Alfvén wave is controlled by Σ_P and Σ_H as explained above. Essentially, the ionospheric electric field is "static" or "inductive" in the two parameter regimes of $\Sigma_P > \Sigma_H$ or $\Sigma_P < \Sigma_H$, respectively. We mainly discuss the ionospheric transmission controlled by the inclination angle and the Alfvén speed profile in the two regimes. In the second part of this chapter, the north-south asymmetry of the ground magnetic perturbations invoked by the asymmetric profile in the magnetosphere-ionosphere system is investigated. Moreover, the effects of the other parameters, the height of the ionosphere and the latitudinal wave number, are also discussed. In Chapter 4, in order to estimate the conjugate asymmetry of the ground magnetic perturbations in the realistic magnetosphere-ionosphere system, it is calculated by using a trapezoid model with the ionospheric and magnetospheric parameters obtained from IRI and IGRF. Then the comparison between the numerical result and the conjugate observations done by Saito *et al.*[1989] and Yumoto [private communication] is shown. In the last section, the results in the present thesis are summarized.

Chapter 2

Model and Basic Equations

2.1 Model

The model used in the present thesis is schematically shown in Fig. 2.1. Latitudinal width of the standing Alfvén oscillation must be considered for numerical analysis of the oscillation in the magnetosphere-ionosphere coupled system (Physically, the ionospheric Hall current makes the Alfvén mode electromagnetic perturbation spread in the horizontal direction in the ionosphere. Further, the pure standing Alfvén oscillation without latitudinal spread [e.g., Poulter and Allan, 1985] does not have the ground magnetic perturbation). Therefore, we need at least a 2D model. In the present thesis, a trapezoid-shape magnetosphere model is used. The model includes the magnetosphere and the infinitely thin ionosphere, which has the height-integrated Pedersen conductivity (Σ_P) and Hall conductivity (Σ_H). While the main magnetic field is assumed to be straight like those in the box model, it is inclined to the ionosphere in the trapezoid model. A free parameter z_0 assigns the magnetic inclination to the ionosphere. Thus, it is possible to investigate the effect of the magnetic inclination on the standing Alfvén oscillation. In addition, the Alfvén speed (V_A) is spatially non-uniform in this model. The spatial profile of V_A is given by

the following equation:

$$V_A(x,z) = \{V_{A,is} - V_{A,eq}(x)\} \left\{ \frac{z}{z_{is}(x)} \right\}^2 + V_{A,eq}(x), \tag{2.1}$$

where $V_{A,is}$ and $V_{A,eq}(x)$ are the Alfvén speed in the ionosphere and that in the equator. z coordinates of the ionosphere is denoted by z_{is}. $V_{A,is}$ is supposed to be constant in each ionospheres. $V_{A,eq}$ monotonically varies with x like

$$V_{A,eq}(x) = V_{A,eq}^{out} \frac{x}{x_{out}} + V_{A,eq}^{in} \frac{(x_{out} - x)}{x_{out}}. \tag{2.2}$$

Here $V_{A,eq}^{out}$ and $V_{A,eq}^{in}$ are the Alfvén speed in the equator of the outer boundary ($x = x_{out}$) and that in the equator of the inner boundary ($x = x_{in} = 0$) (Fig. 2.2). In the present thesis, $V_{A,eq}^{in}/V_{A,eq}^{out} = 4$, $x_{out} = 0.25$, $V_{A,is} = 10$, and the height of the ionosphere (d) $= 0.01$ are chosen unless we specify these values. The numbers of the grid points are 12 in the x direction and 31 in the z direction. V_A is normalized to $V_{A,eq}(x_0)$, where $x_0 = 6x_{out}/11$. We analyze the standing Alfvén oscillation on the field line at $x = x_0$.

2.2 Basic equation and ionospheric boundary conditions

Assuming that the magnetospheric plasma is cold and that the time dependence of the wave field is $\exp(-i\omega t)$, the electric field perturbation perpendicular to the main magnetic field ($\delta \mathbf{E}_\perp$) is governed by the following equation:

$$\frac{\omega^2}{V_A^2(x,z)} \delta \boldsymbol{E}_\perp = \nabla_\perp \times (\nabla \times \delta \boldsymbol{E}_\perp). \tag{2.3}$$

In order to solve this equation as an eigenmode analysis, we adopt the finite difference method. This method requires an orthogonal grid system. Besides, since we use a trapezoid-type magnetosphere model, a mathematical technique should be employed in order to transform the trapezoidal grid system into an orthogonal one. The orthogonal grid system is obtained through the boundary-fitted coordinate technique; the original coordinates, (x, z), is transformed to the boundary-fitted coordinates, (ξ, η), using following

relations:

$$x = \frac{1+\xi}{2} x_{out}, \tag{2.4}$$

$$z = \frac{\eta}{2}(2 + (1+\xi) x_{out} z_0). \tag{2.5}$$

In the (ξ, η) system, the trapezoid model becomes a square shape defined by $|\xi| \leq 1$ and $|\eta| \leq 1$.

The boundary-fitted coordinate technique may be applied to the MHD wave analysis in the dipole model. However, as long as the dipole coordinate system ($\mu = \sin\theta/r^2$, $\nu = \cos^2\theta/r$) is employed, a mesh distribution according to the boundary-fitted coordinates is concentrated around the equator. When the coordinate is transformed in order to be distributed equally along the field line, matrix elements used for the eigenmode analysis happen to have extremely large difference in the magnitude (up to 10^7). Resultantly, numerical calculations do not issue correct eigenvectors. Therefore, this technique does not seem to treat successfully the MHD wave analysis in the dipole magnetosphere-ionosphere-coupled system. This is the reason why we use a simplified trapezoid model.

After Tamao [1984,1986], as the equations of the ionospheric boundary condition, Eqs.(1.8)$\sim$(1.10) are used. However, we need alternate expressions of Eqs.(1.8)$\sim$(1.10) for further numerical analysis. Using the mathematical manipulation similar to that employed by Itonaga *et al.* [1995], we obtain

$$\begin{aligned} & i\omega\mu_0\Sigma_P \nabla\delta\boldsymbol{E}_t + i\omega\mu_0\Sigma_H \hat{N}(\nabla \times \delta\boldsymbol{E}_t) \\ = \quad & -(\hat{N}\hat{z})(\hat{z}\nabla)(\nabla\delta\boldsymbol{E}_\perp) - \left(\tfrac{\omega}{V_A}\right)^2 (\hat{N}_\perp \delta\boldsymbol{E}_\perp), \end{aligned} \tag{2.6}$$

$$\begin{aligned} & i\omega\mu_0\Sigma_P \hat{N}(\nabla \times \delta\boldsymbol{E}_t) - i\omega\mu_0\Sigma_H \nabla\delta\boldsymbol{E}_t \\ = \quad & -\hat{N}(\nabla \times \delta\boldsymbol{E}_\perp)(\nabla\hat{N}) - \hat{N}(\hat{N}\nabla)(\nabla \times \delta\boldsymbol{E}_\perp) + \frac{\hat{N}(\nabla \times \delta\boldsymbol{E}_\perp)}{d}, \end{aligned} \tag{2.7}$$

where $\hat{z}$ is the unit vector along z axis or the main magnetic field. Here $\delta\boldsymbol{E}_t$ is the wave electric field tangential to the ionosphere and $\hat{N}_\perp$ is the tangential component of $\hat{N}$ to the main magnetic field . The ratio of the second term in the r.h.s. of Eq.(2.6) against the first term is estimated as $(\omega/V_A)^2(\hat{N}_\perp\delta\boldsymbol{E}_\perp)/(\hat{N}\hat{z})(\hat{z}\nabla)(\nabla\delta\boldsymbol{E}_\perp) \simeq (l_\perp/l_\parallel)\cot I$ where

$l_{\parallel}$ and $l_{\perp}$ are the field-aligned and latitudinal scales of the standing Alfvén oscillation and I is the inclination angle. Bearing in mind that $l_{\perp} \ll l_{\parallel}$, this ratio is much smaller than 1 unless $I \simeq 0$ (equator). Therefore, the second term is neglected in the present thesis. In addition, the first term in r.h.s. of Eq.(2.7) is vanished in the present model where $\hat{N}$ is uniform. We adopt these equations as the boundary condition for Eq.(2.3).

The magnetic field just below the ionosphere corresponds to that on the ground in the present approximation in which latitudinal width of the wave $> d$. Therefore, the ground magnetic field is derived from Eqs.(1.9) and (1.10) by using $\delta \boldsymbol{E}_t$ obtained from the numerical calculation. We consider the case where the azimuthal wave number (m number) is 0, which means that there is no coupling of the standing Alfvén oscillation and the fast-mode oscillation in the magnetosphere.

Chapter 3

Fundamental Character of the standing Alfvén oscillation in the magnetosphere-ionosphere coupled system

Behaviors of the standing Alfvén oscillation in the trapezoid model is controlled by the three magnetosphere/ionosphere parameters, i.e. the ionospheric conductivity, the magnetic inclination and the field-aligned profile of the Alfvén speed. The ionospheric conductivity directly controls the intensity of the ionospheric electric field associated with the standing Alfvén oscillation. In addition, the ground magnetic perturbation is generated by the Hall current that is the product of the ionospheric electric field and the Hall conductivity. The inclination may change the effective ionospheric conductivity. The field-aligned Alfvén speed profile affects the field-aligned profile of the electric field as well as the eigenfrequency of the standing Alfvén oscillation. Note that the trapezoid model has the straight field line unlike the curved one in the dipole field. The dipole magnetic field has the convergence of the magnetic flux toward the ionosphere. This invokes increase in the electromagnetic field intensity toward the ionosphere. This effect is not

included in the present trapezoid model.

In the former part of this chapter, the ground magnetic perturbation is investigated by using the model in which the magnetosphere and the ionosphere are symmetric with respect to the equator. In the latter part of this chapter, the asymmetric model is employed in order to study the north-south asymmetry of the ground magnetic perturbations invoked by the north-south asymmetry of the magnetosphere-ionosphere system.

At first, we show spatial structures of electric field perturbations associated with the second harmonic standing Alfvén oscillation (δE_x) and that of the fast mode wave (δE_y) generated through the ionospheric Hall current (Fig.2.3). The parameters are $z_0 = 0$, $\Sigma_P = \Sigma_H = 100\Sigma_{A0}$ in the both ionosphere, where $\Sigma_{A0} = 1/\mu_0 V_{A,eq}(x_0)$. Here we normalize Σ_P and Σ_H as

$$\bar{\Sigma}_{P0} = \frac{\Sigma_P}{\Sigma_{A0}}, \qquad \bar{\Sigma}_{H0} = \frac{\Sigma_H}{\Sigma_{A0}}. \tag{3.1}$$

Note that the Alfvén conductance of the second harmonic Alfvén oscillation normalized to Σ_{A0} is about 0.23. Since Σ_P and Σ_H are larger than Σ_{A0} in Fig.2.3, the standing Alfvén oscillation has a node in the ionosphere. Fig.2.4 shows latitudinal profiles of δE_x and δE_y in the ionosphere (top), the magnetic field perturbations (δB_x and δB_y) just above the ionosphere (middle) and those on the ground (bottom). The parameters in Fig.2.4 are as same as those of Fig.2.3. The solid and dotted lines represent x and y components respectively in each panels. From Figs.2.3 and 2.4, it is obvious that the Alfvén mode electric field (δE_x) shows the standing-wave behavior. While δE_y that belongs to the fast mode wave exhibits an evanescent behavior. Note that δB_y on the ground is zero. This is consistent with the theoretical analysis that δB_y on the ground vanishes when m (azimuthal wave number) = 0 [e.g. Nishida, 1978]. Disappearance of δB_y on the ground shown in Fig.2.4 indicates that our numerical calculations have sufficient precision.

We mainly investigate the second harmonic mode of the standing Alfvén oscillation in the present thesis because the magnetic perturbation has an anti-node in the equator.

3.1 North-south symmetric case

In this subsection, we investigate transmission of the magnetic perturbation associated with the standing Alfvén oscillation through the ionosphere in the symmetric model. Hereafter, we use the following notations; $\delta E_{x,is}$ is δE_x in the ionosphere, $\delta E_{x,max}$ is the maximum value of δE_x along the field line, $\delta B_{x,grd}$ is the ground magnetic perturbation, $\delta B_{y,is}$ is δB_y just above the ionosphere and $\delta B_{y,eq}$ is that in the equator (Note that $\delta B_{y,eq}$ of the second harmonic Alfvén oscillation is the maximum δB_y).

3.1.1 Ionospheric conductivity

Yoshikawa *et al.* [1995] already investigated the ionospheric control of the ionospheric electric field associated with the standing Alfvén oscillation. They discussed the importance of Σ_H that yields the inductive electric field from the static one belonging to the Alfvén mode wave. Here, we re-examine their work by addressing the importance of the ionospheric inductive electric field to the ground magnetic perturbations. To do so, conductivity dependences of $\delta E_{x,is}/\delta E_{x,max}$ should be investigated at first. Next, the ground magnetic perturbation ($\delta B_{x,grd}$) compared with the magnetic perturbation just above the ionosphere associated with the standing Alfvén oscillation ($\delta B_{y,is}$) is presented.

In Fig.3.1, we show the ionospheric conductivity control of the electromagnetic field perturbations associated with the standing Alfvén oscillation (δE_x and δB_y). In this figure, two ratios of $\delta E_{x,is}/\delta E_{x,max}$ (Fig.3.1(a)) and $\delta B_{x,grd}/\delta B_{y,is}$ (Fig.3.1(b)) are shown as functions of $\bar{\Sigma}_{H0}$. For each panels, $\bar{\Sigma}_{P0}$ varies from 1 to 1000. Note that the main magnetic field is assumed to be vertical to the ionosphere ($z_0 = 0$) here.

At first, we explain the relation between $\delta E_{x,is}/\delta E_{x,max}$ and $\bar{\Sigma}_{H0}$. Fig.3.1(a) reveals that the ionospheric electric field is controlled by not only $\bar{\Sigma}_{P0}$ but also $\bar{\Sigma}_{H0}$. Yoshikawa and Itonaga [1996] already explained this feature; the ionospheric inductive electric field produced by the Hall current reduces the resultant static field.

Next, we investigate the relation between the ground magnetic perturbation and the

wave magnetic field above the ionosphere ($\delta B_{x,grd}/\delta B_{y,is}$). Fig.3.1(b) indicates that the enhanced Σ_H results in the ionospheric shield effect of the magnetic field perturbation as well as reduction in the ionospheric electric field. Here, let us consider the shield effect of the magnetic field perturbation due to the ionospheric conductivity with a simplified Alfvén wave incident model in a uniform magnetosphere-ionosphere model (V_A, Σ_P, and Σ_H are uniform). Assuming that the Alfvén wave impinges on the ionosphere, we derive the following equation [c.f Appendix]:

$$\frac{\delta B_{x,grd}}{\delta B_{y,is}} = \frac{ik_x}{D\sinh(k_x d)} \frac{\hat{\Sigma}_H}{\hat{\Sigma}_P + k_{||}^A \hat{\Sigma}_H^2 / D}, \tag{3.2}$$

where $\hat{\Sigma}_P = \mu_0 V_A \Sigma_P$, $\hat{\Sigma}_H = \mu_0 V_A \Sigma_H$, $k_{||}^A = \omega/V_A$, $D = k_F + ik_x \coth(k_x d) + k_{||}^A \hat{\Sigma}_P$, $k_F = \sqrt{(\omega/V_A)^2 - k_x^2}$ and k_x is the wave number in the x direction. It is obvious from Eq.(3.2) that the ground magnetic perturbation relative to the magnetic perturbation of the incident Alfvén wave becomes reduced when $\hat{\Sigma}_H$ is much enhanced. This effect found by Tamao [1984] and Fujita [1985] can be called as the magnetic shielding effect due to the ionospheric Hall current. In such enhanced $\hat{\Sigma}_H$ condition, the ionospheric inductive electric field becomes effective and the resultant electric field becomes reduced [Yoshikawa *et al.*, 1995]. Therefore, the enhancement in the inductive electric field in the ionosphere is associated with the magnetic shield effect due to the ionospheric Hall current. Bearing in mind that the two-step procedure of deriving the ground magnetic perturbation employed by Poulter and Allan [1985] and Allan [1995] did not consider Σ_H in the ionospheric boundary condition and thus the magnetic shielding effect due to the ionospheric Hall current does not appear.

For further discussion, we consider here the case where $\hat{\Sigma}_H$ is much smaller than $\hat{\Sigma}_P$. After Yoshikawa and Itonaga [1996], the inductive electric field in the ionosphere is neglected. When the inductive electric field in the ionosphere ($\delta E_{y,atm}^d$) is neglected in the formulations carried out in Appendix, we have

$$\frac{\delta B_{x,grd}}{\delta B_{y,is}} \simeq \frac{ik_x}{D'\sinh(k_x d)} \frac{\hat{\Sigma}_H}{\hat{\Sigma}_P}, \tag{3.3}$$

where $D' = k_F + ik_x \coth(k_x d)$ (This equation is also given by neglecting $k_{||}^A \hat{\Sigma}_H^2 / D$ in the denominator of Eq. (3.2) and $k_{||}^A \hat{\Sigma}_P$ in D). Thus, Eq. (3.3) indicates that, when the ionospheric electric field is static, there is no shielding effect on the ground magnetic perturbation (The condition where the ionospheric electric field is static is referred to as the static condition).

Then we need to specify the upper limit of Σ_H for the static condition. Fig. 3.1 (b) shows that $\delta B_{x,grd}/\delta B_{y,is}$ is proportional to $\bar{\Sigma}_{H0}$ in the case where $\bar{\Sigma}_{H0}$ is smaller. This is the behavior of the standing Alfvén oscillation in the static condition. Whereas, it exceed a certain value (the critical $\bar{\Sigma}_{H0}$), the magnetic shielding effect appears. Detailed investigation of Fig.3.1(b) reveal that the critical $\bar{\Sigma}_{H0}$ is less than or equal to $\bar{\Sigma}_{P0}$.

If $\bar{\Sigma}_{H0}$ exceeds the limit of the static condition, on the contrary, Eq.(3.3) is not valid any longer. When $\hat{\Sigma}_H$ becomes larger ($\hat{\Sigma}_H > \sqrt{D\hat{\Sigma}_P / k_{||}^A}$), Eq.(3.2) becomes

$$\frac{\delta B_{x,grd}}{\delta B_{y,is}} \simeq \frac{ik_x}{k_{||}^A \sinh(k_x d)} \frac{1}{\hat{\Sigma}_H}. \tag{3.4}$$

From this equation, $\delta B_{x,grd}/\delta B_{y,is}$ is inversely proportional to $\hat{\Sigma}_H$. This is the magnetic shielding effect due to the Hall current. When $\hat{\Sigma}_H$ becomes larger, the inductive electric field in the ionosphere is enhanced. Thus, we call this condition where Eq. (3.4) is utilized as the inductive condition from now on. It is characteristic that $\delta B_{x,grd}/\delta B_{y,is}$ is independent of $\hat{\Sigma}_P$ in the inductive condition. Actually, in Fig.3.1(b), $\delta B_{x,grd}/\delta B_{y,is}$ does not depend on $\bar{\Sigma}_{P0}$ when $\bar{\Sigma}_{H0}$ becomes larger.

Here, we have to note that the critical $\bar{\Sigma}_{H0}$ (at which the transition between the static and inductive conditions is occurred) depends on the harmonic number of the standing Alfvén oscillation. From Eq.(3.2), it is expected that the critical $\hat{\Sigma}_H$ for the static condition becomes smaller. This is because an increase in the frequency of the higher harmonic oscillation invokes enhancement of the term of $k_{||}^A \hat{\Sigma}_H^2 / D$ in Eq.(3.2) ($k_{||}^A = \omega / V_A$). Here, we show $\delta B_{x,grd}/\delta B_{y,is}$ of the fundamental, second and third harmonic mode for $\bar{\Sigma}_{P0}$= 10 in Fig.3.2. In fact, we can see that the peak of $\delta B_{x,grd}/\delta B_{y,is}$ for the higher harmonics tends to appear at smaller $\bar{\Sigma}_{H0}$.

3.1.2 Magnetic inclination

Ionospheric transmission of the magnetic perturbation associated with the standing Alfvén oscillation in the static condition exhibits the feature different from that in the inductive condition. Here, we investigate how the behavior of the standing Alfvén oscillation is affected by the magnetic inclination. The ratios of $\delta E_{x,is}/\delta E_{x,max}$ and $\delta B_{x,grd}/\delta B_{y,is}$ are plotted as functions of z_0 in Fig.3.3. The parameters used are $\bar{\Sigma}_{P0}$= 10 and $\bar{\Sigma}_{H0}/\bar{\Sigma}_{P0}$= 0.1, 1, 10 and 100. In Fig.3.3(a), we can see that $\delta E_{x,is}/\delta E_{x,max}$ increase with z_0 in the case of $\bar{\Sigma}_{H0} \leq \bar{\Sigma}_{P0}$ ($\bar{\Sigma}_{H0}$= 1 and 10).

To investigate the effect of the magnetic inclination in detail, Fig.3.4 illustrates the $\bar{\Sigma}_{H0}$-dependence of r_e, which is defined as

$$r_e = \left.\frac{\delta E_{x,is}}{\delta E_{x,max}}\right|_{z_0=1.0} \Big/ \left.\frac{\delta E_{x,is}}{\delta E_{x,max}}\right|_{z_0=0.0}. \tag{3.5}$$

Namely, r_e denotes control of the ionospheric electric field by the magnetic inclination. It is clear from Fig.3.4 that the ionospheric electric field relative to the maximum electric field becomes larger along with the increase in z_0 for $\bar{\Sigma}_{H0}/\bar{\Sigma}_{P0}$= 0.1 and 1 (the static condition), whereas it is almost constant for $\bar{\Sigma}_{H0}/\bar{\Sigma}_{P0}$= 10 and 100 (the inductive condition). This feature is also seen in $\delta B_{x,grd}/\delta B_{y,is}$ shown in Fig.3.3(b). Fig.3.4 presents r_b defined below:

$$r_b = \left.\frac{\delta B_{x,grd}}{\delta B_{y,is}}\right|_{z_0=1.0} \Big/ \left.\frac{\delta B_{x,grd}}{\delta B_{y,is}}\right|_{z_0=0.0}. \tag{3.6}$$

The variation of r_b is essentially the same as that of r_e.

Let us consider further the physical implication of the numerical results. In the case that the ionospheric electric field is static, Allan and Knox [1979b] derived the boundary condition included the effect of the inclination when Σ_H is neglected. They showed that $\hat{\Sigma}_P$ has the factor of $\sin I$ in Eq.(1.10) in the case of $\hat{\Sigma}_H$= 0. Applying this boundary condition to the Eq.(3.3), the following relation equation of $\delta B_{x,grd}/\delta B_{y,is}$ is derived:

$$\frac{\delta B_{x,grd}}{\delta B_{y,is}} \simeq \frac{ik_x}{D' \sinh(k_x d)} \frac{\hat{\Sigma}_H}{\hat{\Sigma}_P \sin I}. \tag{3.7}$$

From Eq.(3.7), r_b is equal to $\sqrt{2}$. In fact, r_b is close to $\sqrt{2}$, for $\bar{\Sigma}_{H0}/\bar{\Sigma}_{P0}$= 0.1 and 1 respectively. On the other hand, it is difficult to manipulate the effect of the inclination

to Σ_H in an analytical way. Therefore, we try to investigate the effect of the magnetic inclination to the behavior of the standing Alfvén oscillation in the inductive condition by using the numerical results. In the range of $\bar{\Sigma}_{H0}/\bar{\Sigma}_{P0}$ for the inductive condition, $\delta B_{x,grd}/\delta B_{y,is}$ in the case of $z_0 = 0$ is led to Eq.(3.4), which shows that $\delta B_{x,grd}/\delta B_{y,is}$ is inversely proportional to $\hat{\Sigma}_H$. If $\hat{\Sigma}_H$ varies with the same rate of the variation of $\hat{\Sigma}_P$, r_b must be equal to $\sqrt{2}$. However, r_b for $\bar{\Sigma}_{H0}/\bar{\Sigma}_{P0}$= 10 and 100 are about 1.13, which shows that the variation of the effect of $\bar{\Sigma}_{H0}$ is smaller than that of $\bar{\Sigma}_{P0}$. This fact implies that the effect of the inclination is not effective in the inductive condition. Consequently, the inclination effectively controls the behavior of the standing Alfvén oscillation only in the static condition.

3.1.3 Equator-ionosphere V_A ratio

We investigate how the behavior of the standing Alfvén oscillation changes according to variation in $V_{A,is}/V_{A,eq}$ ($V_{A,is}$ and $V_{A,eq}$ are the Alfvén speed at the ionosphere and that at the equator on the field line concerned). As noted before, since the trapezoid model has straight magnetic field lines, the flux tube convergence that appears in the magnetosphere is not considered here. Therefore, we consider only the effect of the partial reflection of the Alfvén wave due to increase in V_A along the field line.

Here, Fig. 3.5 shows $\delta E_{x,is}/\delta E_{x,max}$ (Fig.3.5(a)), $\delta B_{x,grd}/\delta B_{y,is}$ (Fig.3.5(b)) and $\delta B_{y,is}/\delta B_{y,eq}$ (Fig.3.5(c)) as functions of $V_{A,is}$. We use $\bar{\Sigma}_{P0}$= 10 and $\bar{\Sigma}_{H0}/\bar{\Sigma}_{P0}$= 0.1, 1, 10 and 100. The main magnetic field is vertical to the ionosphere. Since $\bar{\Sigma}_{P0}$(=10) is larger than the Alfvén conductance (= 1 for $V_{A,is} = 1$ and 0.42 for $V_{A,is} = 10$), δE_x has a node and δB_y has an anti-node in the ionosphere.

It is evident from Fig.3.5(a) and (c) that the electric and magnetic field perturbations normalized to the maximum ones decrease with increase in $V_{A,is}$. This feature can be explained by the partial reflection of the Alfvén wave in the magnetosphere where V_A increases toward the ionosphere along the field line. Note that the flux tube convergence effect counteracts the partial reflection effect in a general magnetosphere condition. When

the field-aligned profile of V_A is controlled by the main magnetic field intensity, the result is modified significantly because of the magnetic flux convergence effect. Whereas, the plasma density profile determines V_A, the present result is invoked.

It is characteristic that $V_{A,is}$-dependence of $\delta B_{y,is}/\delta B_{y,eq}$ is independent of $\bar{\Sigma}_{H0}$ (Fig.3.5(c)). This is because the magnetic field perturbation has an anti-node in the ionosphere. If $\bar{\Sigma}_{P0} < 1$, $\delta B_{y,is}/\delta B_{y,eq}$ must be dependent on $\bar{\Sigma}_{H0}$. On the other hand, the ionospheric electric field decreases along with increase in $\bar{\Sigma}_{H0}$ (Fig.3.5(a)). This feature can be explained by the magnetic shield effect due to the ionospheric Hall current discussed before. Note that this result is independent of the magnetic flux convergence.

Next, $V_{A,is}$-dependence of $\delta B_{x,grd}/\delta B_{y,is}$ shown in Fig.3.5 (b) indicates that $\delta B_{x,grd}/\delta B_{y,is}$ is almost independent of $V_{A,is}$ for $\bar{\Sigma}_{H0}/\bar{\Sigma}_{P0} \leq 1$ (the static condition) and that it decreases against the increase in $V_{A,is}$ for $\bar{\Sigma}_{H0}/\bar{\Sigma}_{P0} > 10$ (the inductive condition). In the static and inductive conditions, $\delta B_{x,grd}/\delta B_{y,is}$ is essentially expressed with Eq. (3.3) and Eq. (3.4), respectively. In addition, increase in $V_{A,is}$ invokes increase in V_A averaged along the field line; this fact yields that larger $V_{A,is}$ leads to smaller Alfvén conductance. Bearing in mind that the ionospheric conductivities appearing in Eqs. (3.3) and (3.4) are normalized to the Alfvén conductance, reduction in the Alfvén conductance associated with increase in $V_{A,is}$ leads to increase in the effective ionospheric conductivity. When $V_{A,is}$ varies from 1 to 10, the mean value of $1/V_A$ along the field line also varies from 1 to 0.42, which is consistent to the variation of $\delta B_{x,grd}/\delta B_{y,is}$. As for the static condition, $\delta B_{x,grd}/\delta B_{y,is}$ is proportional to $\hat{\Sigma}_H/\hat{\Sigma}_P$, which indicates that increase in the Alfvén conductance is not effective. Therefore, $\delta B_{x,grd}/\delta B_{y,is}$ is constant against $V_{A,is}$. On the other hand, in the inductive condition, $\delta B_{x,grd}/\delta B_{y,is}$ is proportional to $1/\hat{\Sigma}_H$. This feature invokes decrease in $\delta B_{x,grd}/\delta B_{y,is}$ associated with increase in $V_{A,is}$. This result is independent of the magnetic flux convergence in a qualitative manner.

3.2 North-south asymmetric case

In the actual magnetosphere-ionosphere coupled system, the ionosphere and magnetosphere are usually asymmetric with respect to the equator. Here, we investigate the north-south asymmetry of the ground magnetic perturbations associated with the standing Alfvén oscillation invoked by the asymmetry of the magnetosphere-ionosphere system.

To begin with, we summarize here the characteristic behavior of the ground magnetic perturbation associated with the standing Alfvén oscillation in the symmetric model.

1. In the static condition ($\Sigma_P > \Sigma_H$), the intensity of the ground magnetic perturbation relative to the magnetic field perturbation just above the ionosphere is proportional to Σ_H/Σ_P. In the inductive condition ($\Sigma_P < \Sigma_H$), it is inversely proportional to Σ_H. The demarcation between the static and inductive conditions is occurred at $\Sigma_H \simeq \Sigma_P$. In addition, when Σ_P is constant, the relative ground magnetic perturbation intensity reaches its maximum at $\Sigma_H \simeq \Sigma_P$.

2. When the main magnetic field has the magnetic inclination (I), the Alfvén wave effectively feels Σ_P reduced by the factor of $\sin I$. Whereas, the effective Σ_H dose not change so much. Thus, the ground magnetic perturbation relative to magnetic perturbation just above the ionosphere is controlled by the inclination angle mainly in the static condition.

3. In the inductive condition, the magnetic field perturbation on the ground divided by that just above the ionosphere decreases along with the increase in the Alfvén speed at the ionosphere level relative to the equatorial one. Whereas, in the static condition, it does not depend on the Alfvén speed at the ionosphere. Further, as long as the trapezoid model is used, the increase in the ionospheric Alfvén speed reduces the wave magnetic field perturbation just above the ionosphere divided by that at the equator due to the partial reflection of the Alfvén wave in the non-uniform profile of the V_A.

4. The higher harmonic standing Alfvén oscillation has the higher eigenfrequency. Therefore, in the inductive condition, the magnetic shielding effect due to Σ_H is enhanced for the higher harmonics. Whereas, in the static condition, the magnetic perturbation on the ground relative to that just above the ionosphere is almost independent of the harmonics.

From now on, we investigate the north-south asymmetry of the ground magnetic perturbations. The symbols "(N)" and "(S)" employed from now mean respectively "in the northern hemisphere (or ionosphere)" and " in the southern hemisphere (or ionosphere)". For example, Σ_P(N) expresses Σ_P in the north ionosphere. Moreover, the symbol of "(N/S)" means the value in the northern hemisphere divided by that in the southern one. For example, $\delta B_{x,grd}$(N/S) expresses $\delta B_{x,grd}(N)$ divided by $\delta B_{x,grd}(S)$.

3.2.1 Ionospheric conductivity

Here, the north-south asymmetry of the electromagnetic field perturbations in the ionosphere and below it due to asymmetry of the ionospheric conductivity is dealt with. In Fig.3.6, $\delta B_{x,grd}$(N/S) is shown as functions of $\bar{\Sigma}_{P0}$(N) and $\bar{\Sigma}_{H0}$(N), respectively. In Fig. 3.6(a) and (b), $\bar{\Sigma}_{P0}$(N) and $\bar{\Sigma}_{H0}$(N) are variables, respectively. Other values of the ionospheric conductivities are 10. Both ionospheres are vertical to the main magnetic field.

It is evident that, from Fig.3.6(a), the ground magnetic perturbation is larger in the hemisphere with smaller $\bar{\Sigma}_{P0}$. This feature can be explained in terms of enhancement of the magnetic shielding effect due to Σ_P in the static condition. In the hemisphere with larger $\bar{\Sigma}_{P0}$, the ionospheric electric field is reduced. Since the ground magnetic perturbation is proportional to the product of the ionospheric electric field and Σ_H, the smaller ionospheric electric field makes the ground magnetic perturbation smaller.

It is characteristic in Fig.3.6(b) that the ground magnetic perturbation in the hemisphere with smaller $\bar{\Sigma}_{H0}$ exceed that in the opposite hemisphere. While, when $\bar{\Sigma}_{H0}$ grows larger than that in the opposite hemisphere, the ground magnetic perturbation in this hemisphere becomes again smaller than that in the opposite hemisphere. In the regime

where $\bar{\Sigma}_{H0}>\bar{\Sigma}_{P0}$ (the inductive condition), the ionospheric electric field is reduced in the hemisphere with larger $\bar{\Sigma}_{H0}$. This effect makes the ground magnetic perturbation in the hemisphere with larger $\bar{\Sigma}_{H0}$ reduced. On the other hand, in the static condition ($\bar{\Sigma}_{H0}(N) < \bar{\Sigma}_{P0}(N) = 10$), $\bar{\Sigma}_{P0}$ which is common in both hemispheres mainly controls the ionospheric electric field. Therefore, the ionospheric electric field intensity is common in the both hemisphere. Since the ground magnetic perturbation in the static condition is proportional to $\bar{\Sigma}_{H0}$, the hemisphere with smaller $\bar{\Sigma}_{H0}$ has the smaller ground magnetic perturbation.

Next, let us consider the north-south asymmetry of the ground magnetic perturbations associated with the fundamental, second, and third harmonic standing oscillations. Fig. 3.7 presents $\delta B_{x,grd}(N/S)$ as a function of $\bar{\Sigma}_{H0}(N)$ in the range of $10 \leq \bar{\Sigma}_{H0}(N) \leq 100$. It is interesting that, in this range of $\bar{\Sigma}_{H0}$, the ground magnetic perturbation in the northern hemisphere is larger than that in the southern one for the fundamental oscillation, whereas this relation is reversed for the second and third harmonics. Let us explain this feature. In this range of $\bar{\Sigma}_{H0}$, the ionospheric condition for the Alfvén oscillation is the transition between the static and inductive conditions. As for the higher harmonics, the eigenfrequency becomes larger; this fact implies that the ionospheric electric field associated with the standing Alfvén oscillation tends to be more inductive for the higher harmonics. Bearing in mind that the ionosphere makes the ground magnetic perturbation smaller in the inductive condition, we can understand that the ground magnetic perturbation is much reduced in the higher harmonics. The present result implies that, in the conjugate observation, north-south intensity relation of a longer-period pulsation (e.g. Pc5 pulsation) is reversed to that of a shorter-period one (e.g. Pc3). As shown later, in the daytime condition, Σ_H is usually larger than Σ_P. In addition, the Alfvén conductance (Σ_A) is usually 10 times smaller than the ionospheric conductivity. Therefore, north-south intensity ratio of the pulsations based on the conjugate ground magnetic observation is likely dependent of the frequency.

3.2.2 Magnetic inclination

The magnetic inclination angle in the ionosphere is sometimes different between the opposite hemispheres. Here, we consider asymmetry of the ground magnetic perturbations when the inclination angles in the both ionospheres are different.

In Fig.3.8, $\delta B_{x,grd}$(N/S) in the cases of $\bar{\Sigma}_{H0} = \bar{\Sigma}_{P0} = 10$ (almost the static condition) and $\bar{\Sigma}_{H0} = 100 = 10\bar{\Sigma}_{P0}$ (the inductive condition) are shown with $z_0(S) = 0.5$. In the case of the static condition, $\delta B_{x,grd}(N/S)$ is nearly proportional to $\sin I$. Since the magnetic inclination (I) reduces Σ_P by $\sin I$, the effective Σ_P ($= \sin I \Sigma_P$) is larger (smaller) in the northern hemisphere for $z_0(N) < z_0(S) = 0.5$ ($z_0(N) > z_0(S)$). As explained above, larger Σ_P reduces the ground magnetic perturbation in the static condition. This is the reason why $\delta B_{x,grd}(N/S)$ is smaller (larger) than 1 for $z_0(N) < z_0(S)$ ($z_0(N) > z_0(S)$). On the other hand, in the.inductive condition ($\bar{\Sigma}_{H0} = 100 = 10\bar{\Sigma}_{P0}$), the inclination does not affect the transmission of the magnetic perturbation across the ionosphere. Namely, the previous calculations on the influence of the inclination on the transmission indicated that the effective Σ_H is not so dependent on the inclination angle. Thus, $\delta B_{x,grd}(N/S)$ is almost constant against $z_0(N)$ in the inductive condition.

3.2.3 Equator-ionosphere V_A ratio

It is usual that the field-aligned profile of V_A is asymmetric with respect to the equator. Here, let us investigate how the north-south asymmetry of the field-aligned variation in V_A affects the asymmetry of the ground magnetic perturbations. The present model assumes the field-aligned profile of V_A defined with Eq. (2.1). Thus, the larger $V_{A,is}$ indicates that the field-aligned profile of $V_{A,is}$ becomes rapidly larger toward the ionosphere. The main magnetic field is vertical to the ionosphere.

Fig.3.9 shows $\delta B_{x,grd}(N/S)$ as a function of the ionospheric V_A in the northern hemisphere (denoted with $V_{A,is}(N)$) in the case where $V_{A,is}(S) = 10$ as well as $\bar{\Sigma}_{P0} = \bar{\Sigma}_{H0} = 10$ in both ionospheres. This figure indicates that the ground magnetic perturbation becomes larger in the hemisphere where $V_{A,is}$ is smaller. (Note that $\delta B_{x,grd}(N/S) = 1$ at

$V_{A,is}(N) = 10 = V_{A,is}(S)$.) This feature is interpreted as follows; at first, partial reflection of the Alfvén wave due to spatial increase in V_A along the field line reduces the electric field perturbation of the Alfvén wave toward the ionosphere. Then the larger $V_{A,is}$ invokes the smaller ionospheric electric field perturbation associated with the Alfvén wave. Thus, the ground magnetic perturbation, which is the product of the ionospheric electric field and Σ_H, becomes smaller in the hemisphere with larger $V_{A,is}$.

Note that asymmetry of V_A in the actual magnetosphere is produced both by the asymmetry of the main magnetic field intensity and by that of the plasma density. The former associates with convergence of the magnetic flux in the magnetosphere. This convergence may yield intensification of the electromagnetic field perturbation in the hemisphere with larger main magnetic field intensity. V_A is larger in this hemisphere as long as the plasma density is not so different in both hemispheres. On the other hand, the partial reflection effect yields smaller electromagnetic field perturbation in the hemisphere with larger V_A. Therefore, the both effects counteract each other. The present thesis does not consider the magnetic flux convergence effect. This effect yields the north-south magnetic field intensity ratio independent of season. On the other hand, when the V_A profile is assumed to be derived from the plasma density, it shows the seasonal variation because of seasonal variation of the plasma density in the lower magnetosphere. Then, the north-south asymmetry due to the partial reflection effect exhibits the seasonal variation with a bias (The partial reflection effect can have the bias part in the asymmetry when the north-south asymmetry of $V_{A,is}$ has a bias). Therefore, in the actual magnetosphere, the north-south asymmetry controlled by the equator-ionosphere V_A ratio will have the two features; one is the bias that derived from the flux tube convergence effect and the partial reflection effect, and another is the seasonal variation from the partial reflection effect. When the partial reflection effect may overcome the flux tube convergence one, the bias part in the north-south asymmetry is qualitatively consistent with the present numerical results. This depends on the field-aligned profile of V_A.

3.3 The latitudinal wave number and the height of the ionosphere

By now, we investigate how the ground magnetic perturbation is affected by the ionospheric conductivity, the inclination, and Equator-Ionosphere V_A ratio. However, Eq. (3.2) indicates that other parameters also affect the ground magnetic perturbation; these are the latitudinal wave number (k_x) and the height of the ionosphere (d). Although these are not quantities varying according to the natural condition, we check here the effects due to these quantities. Here, let us consider how variations of k_x and d affect the ionospheric electric field (say, static or inductive) because this classification is essentially important for assessing the north-south asymmetry of the conjugate ground magnetic perturbations.

At first, we briefly consider the latitudinal width of the toroidal oscillation. Strictly speaking, the pure standing Alfvén oscillation does not have the latitudinal width. However, such oscillation has no magnetic effect on the ground because of severe spatial attenuation in the neutral atmosphere [Hughes and Southwood, 1976a]. Only the Alfvén wave coupled with the fast magnetosonic mode wave has its latitudinal width [Southwood, 1974]. However, it is still quite difficult to treat self-consistently the interaction between the coupled oscillation and the anisotropic conducting ionosphere. Bearing in mind that the behavior of the oscillation at the resonant field line is almost Alfvénic, we considered the ionosphere-Alfvén wave interaction as a working model for ground-based observations. Therefore, the latitudinal width is assigned here as a parameter. As similar to the case of d, it is possible to investigate the effect of the latitudinal width ($\simeq 1/k_x$) based on Eqs. (3.2)-(3.4). As for the disturbances with the latitudinal extent larger than d, we can see that k_x almost disappears for $k_x d \ll 1$. This fact indicates that the variation of k_x ($\simeq$1/latitudinal width) has no significant influence on the ionospheric electric field.

In the present thesis, we use d (the height of the ionosphere normalized to the half-length of the field line) = 0.01. When the actual height of the ionosphere is assumed to be about 100km, the length of the magnetic field line is 20,000km which corresponds to

L≃3. However, the normalized d should not be a fixed value since the magnetic field line is not constant along the latitude. In the higher latitudes ($L > 3$), d smaller than 0.01 should be assigned. In Fig. 3.10, the dependence of the ground magnetic perturbation on the Hall conductivity for various values of d is shown. It is clearly shown that, when d becomes smaller (say, the case of the higher latitude), the effect of the inductive effect becomes weaker. Thus the ground magnetic perturbation becomes larger. In fact, Eqs. (3.2)-(3.4) indicate that smaller d reduces the inductive electric field. Therefore, we can conclude that the magnetic shielding effect due to the ionospheric Hall current tends to appear in the more enhanced Hall conductivity. From Eqs. (3.2)-(3.4), we also find that smaller d enhances the ground magnetic perturbation. In evaluating latitudinal variations in the conjugate asymmetry of the ground magnetic perturbations in the latter part of this section, d is adjusted to the field line length at the relevant latitude.

Chapter 4

North-south asymmetry of the ground magnetic perturbations in the realistic model

In previous chapters, parameter-dependence of the ground magnetic perturbation associated with the standing Alfvén oscillation has been considered. Physical explanation of the numerical results was the main target in the previous chapter. Implication of the present thesis in the actual phenomena is now considered. Therefore, by using the realistic quantities of the ionospheric conductivity, the magnetic inclination, the field-aligned profile of V_A and the height of the ionosphere (d), we intend to evaluate asymmetry of the ground magnetic perturbations at the conjugate points. Note that the present model employs the straight magnetic field, which is different from the actual dipole magnetic field. Consequently, the results are not always corresponding to the observed one. However, we can find some important features of the north-south asymmetry of the ground magnetic perturbations by using the present model calculation. Ignorance of the magnetic field curvature is briefly discussed in the last part of this section.

We calculate the asymmetries at 12 points for three values of L (= 2, 4 and 6) and 4 magnetic longitudes ($\Phi = 0°$, $90°$, $180°$ and $270°$).

4.1 Assignment of the realistic physical values

We explain how to derive the realistic values of the parameters. As concerns the Alfvén speed at the ionospheric altitudes ($V_{A,is}$), the north-south asymmetry of the plasma density and that of the magnetic field intensity should be taken into consideration. For the plasma density, we use IRI90. Bearing in mind that the MHD oscillation with long wavelength feels V_A averaged along the field line, only the plasma density at altitudes around 100km does not contribute to $V_{A,is}$ that is felt by the MHD oscillation. Therefore, the ion density averaged in the region from 100 to 2000km is assumed to contribute to $V_{A,is}$. IGRF95 is used for the magnetic field intensity. Then, $V_{A,is}(\mathrm{N})$ and $V_{A,is}(\mathrm{S})$ are given by

$$V_{A,is}(\mathrm{N}) = V_{A,eq} L \sqrt{1+3\cos\theta_L} \frac{2B_0(\mathrm{N})}{B_0(\mathrm{N})+B_0(\mathrm{S})} \frac{\sqrt{\rho(\mathrm{N})}+\sqrt{\rho(\mathrm{S})}}{2\sqrt{\rho(\mathrm{N})}}, \tag{4.1}$$

$$V_{A,is}(\mathrm{S}) = V_{A,eq} L \sqrt{1+3\cos\theta_L} \frac{2B_0(\mathrm{S})}{B_0(\mathrm{N})+B_0(\mathrm{S})} \frac{\sqrt{\rho(\mathrm{N})}+\sqrt{\rho(\mathrm{S})}}{2\sqrt{\rho(\mathrm{S})}}, \tag{4.2}$$

where θ_L, B_0, ρ are respectively the colatitude of the foot point of an L-shell, the total magnetic intensity at the ionosphere derived from IGRF95, and the plasma density derived from IRI90. The values of $V_{A,is}$ is shown in Table 4.1. The variation of V_A along the field line is proportional to z^2 as shown in Eq. (2.1).

The inclinations are also derived from IGRF95. The values of z_0 ($z_0 = 1/\tan I$) are listed in Table 4.2.

IRI90 and CIRA72 are used for calculation of the height-integrated ionospheric conductivity. The integration range is from 80 to 180km. This range includes the peak in the height profile of the ionospheric conductivity. The values of Pedersen and Hall conductivities in the upper boundary become smaller than one third of each peak values. We also employ 100 of the sunspot number because this value is roughly the averaged sunspot number ($0 \sim 200$). Note that variation in the height-integrated conductivity against sunspot number change from 50 – 150 is smaller than 20%. The local time is assigned as 12LT because Pc pulsations are mainly observed in the daytime. To investigate the seasonal dependence, the conductivities in the equinox and solstice seasons (March,

June, September, and December) are calculated.

To obtain the normalized ionospheric conductivity that is necessary in the present calculation, we need values of the Alfvén speed in the equator ($V_{A,eq}$) of each L-shells. These values are derived from comparisons between the observational eigenfrequencies as listed in Table 2 and calculated ones. Bearing in mind that the eigenfrequency of the standing Alfvén oscillation depends on the ionospheric conductivity and the Alfvén conductance, we need to specify these two conductivities in the observations. Samson *et al.* [1972] analyzed Pc 4 and Pc 5 events in Canadian chain ($L \geq 4$) during northern summers of two years. The conductivity of the southern conjugate ionosphere is probably smaller than the Alfvén conductance of the field line at L = 6 because the ionosphere is located in the dark hemisphere (Actually, the present procedure yields 0.16S of the ionospheric conductivity and 0.35S of the Alfvén conductance). In the northern ionosphere, the conductivity becomes larger than the Alfvén conductance. Thus, the standing Alfvén oscillation can be regarded to have an anti-node of the electric field perturbation in the southern ionosphere and a node in the northern ionosphere. Thus, the fundamental standing Alfvén oscillation in $L = 6$ may become the quarter-wave mode [Allan and Knox, 1979a]. In order to obtain $V_{A,eq}$ of $L = 6$, we calculate the eigenfrequency by using the ionospheric conductivities larger than the Alfvén conductance (e.g., $\bar{\Sigma}_{P0} = \bar{\Sigma}_{H0} =$ 1000) in the north ionosphere and the conductivities smaller than it (e.g., $\bar{\Sigma}_{P0} = \bar{\Sigma}_{H0}$ =0) in the south ionosphere. At L-shells of $L = 2$ and 4, the standing Alfvén oscillations seem to have nodes of the electric field perturbations in the both ionospheres. Thus, the eigenfrequency calculated with large ionospheric conductivities in the both ionospheres is compared with the observed frequency. Note that $V_{A,eq}$ thus evaluated are 1,090km/s, 990km/s and 1,250km/s for $L = 2$, 4 and 6, respectively. Those values seem realistic. The normalized ionospheric conductivity is listed in Table 3.

The height of the ionosphere (d) is normalized to the length of the field line. Since this height is 100km, the value of d is 0.0176, 0.0065 and 0.004 for L=2, 4 and 6, respectively.

4.2 Characteristic features of asymmetry of the conjugate ground magnetic perturbations

Fig.4.1 shows seasonal variations of $\delta B_{x,grd}$(N/S) associated with the three harmonics at 12 points. The following features are evident from this figure;

1. $\delta B_{x,grd}$(N/S) for the second and third harmonics become smaller in the summer hemisphere than in the winter hemisphere. $\delta B_{x,grd}$(N/S) for the fundamental mode is almost constant except $\Phi = 0°$ and $\Phi = 180°$ at $L = 6$.

2. At $L = 4$ and 6, the seasonal variations of $\delta B_{x,grd}$(N/S) at $\Phi = 90°$ are similar to that at 270°, while that at $\Phi = 0°$ is different from that at 180°. Especially in solstice seasons, $\delta B_{x,grd}$(N/S) at $\Phi = 0°$ is the smallest, and that at $\Phi = 180°$ is the largest. Those at $\Phi = 90°$ and 270° are in between. On the other hand, the longitudinal variation at $L = 2$ shows the behavior different from that at $L = 4$ and 6. Namely, at $L = 2$, $\delta B_{x,grd}$(N/S) is largest at $\Phi = 90°$ and smallest at Φ=270°.

The first feature gives a hint for specifying the condition of interaction between the ionosphere and the MHD oscillation, namely, the static condition or the inductive one. In the inductive condition, $\delta B_{x,grd}/\delta B_{y,is}$ is proportional to $1/\Sigma_H$. In order to investigate $\delta B_{x,grd}$(N/S), we need to check $\delta B_{y,is}$(N/S). Since Σ_P is larger than the Alfvén conductance at 12LT, $\delta B_{y,is}$ has an anti-node in the ionosphere. This indicates that $\delta B_{y,is}$(N/S) does not change so significantly associated with variation of the ionospheric conductivity. Therefore, under the inductive condition, $\delta B_{x,grd}$ is regarded to be proportional to $1/\Sigma_H$ at the ionosphere in the relevant hemisphere. As Σ_H in the summer is larger than that in the winter, Σ_H(N/S) reaches maximum in June and minimum in December. This variation of Σ_H yields seasonal variation of $\delta B_{x,grd}(N/S)$; it is larger in winter and smaller in summer. This variation is consistent to that of $\delta B_{x,grd}$ of the second and third harmonics shown in Fig.4.1. In the static condition, on the other hand, $\delta B_{x,grd}$ is proportional to Σ_H/Σ_P. As Σ_H/Σ_P is almost constant during a year, $\delta B_{x,grd}$ does not vary so much.

Consequently, only the ionospheric electric field associated with the fundamental mode is static, whereas, those of the higher harmonics are inductive (Note that the explanation is valid when the ionospheric conductivity is larger than the Alfvén conductance).

The results described above indicate that the two-step procedure of evaluating the ground magnetic perturbation [Allan, 1995] is valid for the fundamental mode oscillation because the ionospheric electric field is almost static. As for the higher harmonics, we need to treat the interaction between the MHD wave and the anisotropic conducting ionosphere with the self-consistent manner.

The seasonal variation of the asymmetry for the fundamental mode exhibits anomalous behaviors at $\Phi = 0°$ and 180° at $L = 6$. The exceptionally enhanced asymmetry for the fundamental mode at $L = 6$ is explained by the difference of the ionospheric conductivities at conjugate ionospheres. This difference of the conductivities is associated with the difference between the geomagnetic and geographic coordinates. For example, in June, the ionosphere is almost daytime condition in the Northern Hemisphere and nighttime condition in the Southern Hemisphere at $\Phi = 0°$. Therefore, the asymmetry of the ionospheric conductivities between the conjugate points at $\Phi = 0°$ is quite intensified. Note that the conductivity in the south ionosphere falls in less than the Alfvén conductance. Whereas, that in the north ionosphere is larger than the Alfvén conductance. Then, the electric field associated with the standing Alfvén oscillation has an anti-node in the south ionosphere and a node in the north ionosphere (the quarter wave). Therefore, $\delta B_{x,grd}(\mathrm{S})$ becomes much smaller than $\delta B_{x,grd}(\mathrm{N})$. Thus $\delta B_{x,grd}(\mathrm{N/S})$ of the fundamental mode becomes larger in June at $\Phi = 0°$. The anomalous seasonal variation of the asymmetry does not appear at $L = 4$ because the ionospheric conductivity is not small to make the mode in the ionosphere an anti-node.

Let us investigate the longitudinal change in seasonal variation of $\delta B_{x,grd}(\mathrm{N/S})$ (the second feature). It seems curious that seasonal variation of $\delta B_{x,grd}(\mathrm{N/S})$ depends on longitude. Thus, we consider the reason. This is again attributed to the difference between the geographic and geomagnetic coordinates. Namely, the conjugate points at $\Phi = 90°$

and at 270° lie in the almost same distance from the geographic equator. At $\Phi = 0°$ and at 180°, on the other hand, the conjugate points shift southward and northward, respectively. The effect of this shift is notable in solstice seasons at $L = 4$ and 6. In June, Σ_H(N/S) increases at $\Phi = 0°$ and decrease at $\Phi = 180°$. As $\delta B_{x,grd}$ of the second and third modes are proportional to $1/\Sigma_H$, $\delta B_{x,grd}$ at $\Phi = 0°$ is smaller and that at $\Phi = 180°$ is larger. On the other hand, the longitudinal variation of $L = 2$ is different from those at $L = 4$ and 6. This may be attributed to the fact that the regional anomaly in the ionospheric conductivity in the Brazilian anomaly invokes a peculiar seasonal variation of the conjugate ground magnetic perturbations at $L = 2$.

4.3 Comparison with observations

There are several works that analyzed the conjugate asymmetry of the ground magnetic perturbations done by Saito *et al.* [1989] and Yumoto [private communication]. In this section, we compare these observations and the numerical results.

4.3.1 Comparison with the observation of 210° magnetic meridian chain

First, we compare the present study with the results which carried out ground-based magnetic observation campaign (the 210° MM observation [Yumoto *et al.*, 1992]). In this campaign, H-components of Pc pulsations at conjugate pairs are analyzed in order to investigate the north-south asymmetries of the Pc3-5 powers in higher (L~5.4) and lower (L~1.6) latitudes [Yumoto, private communication]. These data are obtained in north summer season (1993/6-8) and north winter season (1993/12-1994/2) for each stations [c.f. Table 4.5]. After Yumoto's analysis, Pc3 power at lower latitude and Pc4-5 power at higher latitude are larger in the hemisphere with smaller main magnetic intensity (KOT>MCQ, MSR>BRV) [Table 4.6]. He also revealed that Pc3 power at higher latitude is larger in the winter hemisphere than in the summer hemisphere.

Let us compare the observed results with the present numerical ones. We see first the higher-latitude observation (KOT-MCQ pair). The magnetic inclination at KOT is almost the same as that at MCQ. Thus, the asymmetry of $\delta B_{x,grd}$ is caused by those of the conductivity and the Alfvén speed. In these latitudes, the longer-period pulsations (Pc4-5) may be regarded as the fundamental oscillation. This oscillation has the static electric field in the ionosphere. In static condition, as describe before, $\delta B_{x,grd}$ is proportional to Σ_H/Σ_P when $\Sigma_P > \Sigma_A$. From our estimation, Σ_P in KOT and MCQ are larger than Σ_A in both seasons. Thus Σ_H/Σ_P(KOT/MCQ) is proportional to the asymmetry of $\delta B_{x,grd}$(KOT/MCQ) due to the ionospheric conductivity. As $\delta B_{y,is}$ decreases with $V_{A,is}$, moreover, $V_{A,is}$(KOT/MCQ) tells the asymmetry of $\delta B_{x,grd}$ due to the Alfvén speed. By evaluating ionospheric parameters with the procedure same as that employed for the numerical calculation, we have 0.98 (< 1) of Σ_H/Σ_P(KOT/MCQ) in north summer and 1.07 (> 1) in north winter. Besides, $V_{A,is}$(KOT/MCQ) is smaller than 1 in both season. These evaluations suggest $\delta B_{x,grd}$(KOT/MCQ) > 1 in north winter case as long as the trapezoid model is employed. In north summer, Σ_H/Σ_P(KOT/MCQ) < 1 and $V_{A,is}$(KOT/MCQ) < 1 but $V_{A,is}$(KOT/MCQ) is much smaller than Σ_H/Σ_P(KOT/MCQ). Thus, the result based on the trapezoid model indicates $\delta B_{x,grd}$(KOT/MCQ) > 1. Therefore, this evaluation is consistent with the observation. For the higher harmonics (Pc3) with the inductive ionospheric electric field, $B_{x,grd}$ may be larger in the winter hemisphere because smaller Σ_H in the winter hemisphere at KOT and MCQ reduces the shielding effect due to the ionospheric Hall conductivity. Thus, in both cases of longer- and shorter-period oscillations, our study is consistent to the results observed in higher latitude obtained in the 210° MM observation. This fact may indicate that the convergence of the flux tube does not so effective in this event.

In the last, let us consider the asymmetry observed in the lower latitude in the 210° MM observation campaign. Pc3 corresponds to the fundamental mode. Σ_H/Σ_P(MSR/BRV) and $V_{A,is}$(MSR/BRV) are 1.00 and 0.93 in the north summer and 0.91 and 1.04 in the north winter, respectively. Note that the inclinations of both stations are also almost

same. From these values, the present calculation suggests that $\delta B_{x,grd}$(MSR/BRV) of the fundamental mode is larger than 1 in north summer and smaller than 1 in north winter. This result is consistent to the observational study in north summer, whereas not consistent in north winter. This discrepancy does not disappear when we use the dipole magnetosphere model because the flux tube convergence tends to yield larger magnetic intensity in the hemisphere with larger main magnetic field intensity. We need to enhance the effect of the partial reflection of the Alfvén wave by the field-aligned increase in V_A in order to obtain the result consistent with the observation. We need more realistic model of V_A along a field line in addition to employment of the dipole model. Further, validity of the thin-ionosphere assumption should be re-considered when the lower-latitude phenomena are treated.

4.3.2 Comparison with the observation of Syowa-Iceland conjugate stations

Saito *et al.* [1989] investigated the seasonal variation of the H component power of Pc 3-5 pulsations at the Syowa-Iceland conjugate stations [c.f Figure 4.2]. They revealed that, in the solstice seasons, the Pc 3-5 pulsation power is stronger in the winter hemisphere than in the summer hemisphere in the whole range of the frequency. This does not coincide with the Pc 4-5 pulsation power ratio obtained from the 210° MM higher-latitude pair (KOT-MCQ). They also reported that the power ratio is less than 0.6 dB in Syowa-Iceland pair. (Note that the 210° MM observations do not issue the quantitative power ratio.) In order to check that our model can explain this observational result, we calculate the asymmetry of the ground magnetic perturbation [Figure 4.3] by using the parameters on IGRF95 and IRI90 [Table 4.9]. The parameters at the 1200UT condition are used.

The numerical results shown in Figure 4.3 indicate that the ground magnetic perturbations are larger in the winter hemisphere. Since the 2nd and 3rd harmonic oscillations are likely to have the inductive ionospheric electric field, the ground magnetic perturbation tends to be inversely proportional to Σ_H. Referring to Table 4.9, we notice Σ_H much

smaller in the winter hemisphere. Therefore, the ionospheric shielding effect due to the Hall current becomes a dominating mechanism in determining the conjugate asymmetry in the ground magnetic field perturbation. Finally, the ground magnetic perturbation should become larger in the winter hemisphere as obtained in our model calculation [Figure 4.3].

Bearing in mind that the fundamental mode oscillation is likely to have the static ionospheric electric field, Σ_H/Σ_P should be checked for investigating the asymmetry. Compared to the case of Σ_H, the conjugate asymmetry in Σ_H/Σ_P is not so enhanced. Thus, we need to consider the effect from the asymmetry in $V_{A,is}$ as well. The highly enhanced asymmetry in Σ_H may invoke non-negligible effect on the ground magnetic perturbation associated with the Pc 4-5 pulsations. Existence of these competitive mechanisms requires a numerical calculation. The numerical result shown in Figure 4.3 reveals that the ground magnetic perturbation of the fundamental mode oscillation is again larger in the winter hemisphere. This numerical result is qualitatively consistent to the result from Syowa-Iceland conjugate observations. Therefore, the discrepancy in the seasonal variation in the conjugate magnetic perturbation intensity between the two observations may come from difference in the ionospheric and magnetospheric physical conditions.

In spite of the qualitative agreement between the observation and the model, there is quantitative disagreement because the Syowa-Iceland observation (0.6 dB = 1.07 of the asymmetry) reported the asymmetry much smaller than the present numerical calculation does [Figure 4.3]. As the reason of the disagreement, over-simplification of the model magnetosphere can be pointed out. To resolve this disagreement, we have to study with more realistic model. However, as long as the standing Alfvén oscillation model is employed, the extremely enhanced asymmetry in the ionospheric conductivity like Syowa-Iceland conjugate pair seems to invoke considerably large asymmetry in the ground magnetic field. There may be still new physics on the mechanism determining the ground magnetic perturbation associated with the standing Alfvén oscillation. In addition to re-assessment of the theory, we believe that the observational results should be again carefully checked. We hope the 210° MM observation will give us quantitative results on the asymmetry.

Chapter 5

Conclusion and Summary

We investigate the standing Alfvén oscillation of the magnetic field line by using a model magnetosphere with the anisotropically conducting ionosphere. In this model, the main magnetic field line is straight and has an arbitrary inclination angle to the ionosphere. At first, the general features of the ground magnetic perturbation associated with the standing Alfvén oscillation are considered in the static condition of the ionosphere conductivity ($\Sigma_P > \Sigma_H$) and in the inductive one ($\Sigma_P < \Sigma_H$). Here, effects of the ionospheric conductivity, inclination angle and the Equator-ionosphere V_A ratio are investigated. The main results are summarized as follows.

1. In the static condition, the intensity of the ground magnetic perturbation normalized to the magnetic perturbation just above the ionosphere is proportional to Σ_H/Σ_P. In the inductive condition, it is proportional to $1/\Sigma_H$.

2. The magnetic inclination controls the ground magnetic perturbation normalized to the magnetic perturbation just above the ionosphere mainly in the static condition.

3. The intensity of the ground magnetic perturbation normalized to the magnetic perturbation just above the ionosphere decreases with the Alfvén speed in the ionosphere mainly in the inductive condition.

4. For the higher altitude of the ionosphere, the ionospheric electric field becomes inductive and the ground magnetic perturbation becomes smaller.

Next, we study the asymmetry of the ground magnetic perturbations at geomagnetically conjugate points invoked by north-south asymmetries of the above three parameters. The features of the ground magnetic perturbations are also considered in static and inductive conditions. The main results are as follows.

1. When Σ_H in the both ionospheres have the same value, the ground magnetic perturbation is larger in the hemisphere with smaller Σ_P. When the both hemispheres have the same value of Σ_P, it is larger in the hemisphere with larger Σ_H in the static condition and smaller in the hemisphere with smaller Σ_H in the inductive condition.

2. In the static condition, the ground magnetic perturbation is larger in the hemisphere with smaller inclination. In the inductive condition, on the other hand, the ground magnetic perturbations in the both hemispheres are same even if the inclination angles are different.

3. The ground magnetic perturbation is larger in the hemisphere with the smaller Alfvén speed in the ionosphere due to the partial reflection of the Alfvén wave within the trapezoid model that does not have a curved magnetic field. This partial reflection effect is counteracted by the magnetic flux convergence associated with the dipole magnetic field, although this effect is excluded in the present model.

It should be noted on the third result described above. Namely, the north-south asymmetry of the ground magnetic perturbations derived from the partial reflection mechanism may invoke seasonal variation because V_A is affected not only by the main magnetic field intensity but also by the plasma density that exhibits seasonal variation. On the other hand, the magnetic flux tube convergence effect invokes a DC bias in the asymmetry independent of season.

The height of the ionosphere and the latitudinal wave number also affect the ground magnetic perturbations. As the latitudinal wave number is assigned parameter, the dependence of the ground magnetic perturbation on the height of the ionosphere is investigated. Its effect is listed as follow.

1. When the height of the ionosphere is larger, the ionospheric electric field becomes inductive. This implies that the inductive effect is larger in the lower latitude.

In the last part of the present thesis, we evaluate asymmetry of the conjugate ground magnetic perturbations by using the ionospheric conductivity based on the IRI model as well as the field-aligned V_A profile and magnetic inclination based on the IGRF model. The magnetic flux convergence effect that is excluded in the present trapezoid model is qualitatively discussed. The results are as follows.

1. The calculation based on realistic ionospheric parameters reveals that the fundamental mode has the static electric field in the ionosphere. Therefore, the two-step procedure of obtaining the ground magnetic perturbation from the standing Alfvén oscillation [Allan, 1995] is valid for the fundamental mode. On the other hand, the higher harmonic modes have the inductive one. The Hall conductivity plays an essential role in the ionospheric reflection and transmission of the standing Alfvén oscillation.

2. The north-south asymmetry of the ground magnetic perturbations depends on not only the L-value but also the magnetic longitude; this is because the ionosphere and magnetic field conditions are not uniform along the longitude.

3. Our model and parameter estimation can explain the north-south asymmetries observed by the 210° MM chain and Syowa-Iceland conjugate stations. Quantitatively speaking, however, numerical estimation of the asymmetry in Syowa-Iceland stations is not in complete agreement with the observation.

The model used here is still quite artificial. The present trapezoid model ignores the curvature of the main magnetic field that is at least a dipole magnetic field. When

the curvature is taken into account, decrease in the magnetic flux toward the ionosphere may concentrate the electromagnetic field perturbation associated with the Alfvén wave propagating toward the ionosphere. We need to employ the dipole magnetosphere model in the next study.

Only the stationary standing Alfvén oscillation is considered in the present thesis. Note that this is also quite idealized model of the actual phenomena. In the actual phenomena, we need to take into account another physical mechanisms (for example, the phase mixing effect) when we try to compare the observed data and the present numerical results. However, it seems interesting to compare the numerical results with observed ones by evaluating the magnetospheric magnetic perturbation from the ground magnetic perturbation. The ground observation is now continuously carried out in a network base. Combination of the ground-based observation and the quantitative numerical model should open a new stage of the research.

Appendix A

Transmission of the Alfvén Wave through the Ionosphere

The z axis is parallel to the main magnetic field and vertical to the ionosphere($z = -d$) and the ground ($z = 0$). The Alfvén velocity is spatially uniform and azimuthal wave number (m) is 0. Supposing that the time dependence of the wave field is $\exp(-i\omega t)$, the parallel wave number of Alfvén wave($k_{\parallel}^{A}$) is ω/V_A. Then the electric field of Alfvén wave in the magnetosphere is given by

$$\delta E_x = \delta E_x^i e^{ik_{\parallel}^{A}(z+d)} + \delta E_x^r e^{-ik_{\parallel}^{A}(z+d)}, \tag{A.1}$$

where the first and second terms of r.h.s. represent the incident (with the suffix ^{i}) and reflected (with the suffix ^{r}) waves. The fast mode wave is produced in the ionosphere due to the Hall current. The wave number of fast mode wave is $k_F = \sqrt{k_{\parallel}^{A\,2} - k_x^2}$. Then the electric field of the fast mode wave is given by

$$\delta E_y = \delta E_y^r e^{-ik_F(z+d)} \tag{A.2}$$

where δE_y^r is electric amplitude of the fast mode wave. From Eqs.(A.1) and (A.2), the magnetic fields of the Alfvén wave and fast mode wave are given by

$$\delta B_y = \frac{1}{V_A}\delta E_x^i e^{ik_\parallel^A(z+d)} - \frac{1}{V_A}\delta E_x^r e^{-ik_\parallel^A(z+d)}, \tag{A.3}$$

$$\delta B_x = \frac{k_F}{\omega}\delta E_y^r e^{-ik_F(z+d)}. \tag{A.4}$$

Next, the electric fields of the waves in the neutral atmosphere are given by

$$\delta E_{x,atm} = \delta E_{x,atm}^d e^{i\rho z} + \delta E_{x,atm}^u e^{-i\rho z}, \tag{A.5}$$

$$\delta E_{y,atm} = \delta E_{y,atm}^d e^{i\rho z} + \delta E_{y,atm}^u e^{-i\rho z}. \tag{A.6}$$

As the frequency is so low, the wave number of waves in the atmosphere is

$$\rho^2 = \left(\frac{\omega}{c}\right)^2 - k_x^2 \simeq -k_x^2. \tag{A.7}$$

Moreover, since the electric field tangential to the ground is zero in the ground, we have

$$\delta E_{x,atm} = \delta E_{x,atm}^d (e^{-k_x z} - e^{k_x z}), \tag{A.8}$$

$$\delta E_{y,atm} = \delta E_{y,atm}^d (e^{-k_x z} - e^{k_x z}), \tag{A.9}$$

and the magnetic fields are

$$\delta B_{x,atm} = \delta E_{y,atm}^d \left(\frac{k_x}{i\omega}\right)(e^{-k_x z} + e^{k_x z}), \tag{A.10}$$

$$\delta B_{y,atm} = 0. \tag{A.11}$$

Here Eq.(A.11) is derived from $j_z = 0$ [c.f. Nishida, 1978].

The ionospheric boundary conditions are given by Eqs.(1.8)$\sim$(1.10). From Eq.(1.8), we have

$$\delta E_x = \delta E_{x,atm}, \tag{A.12}$$

$$\delta E_y = \delta E_{y,atm}, \tag{A.13}$$

thus

$$\delta E_x^i + \delta E_x^r = \delta E_{x,atm}^d (e^{k_x d} - e^{-k_x d}), \tag{A.14}$$

$$\delta E_y^r = \delta E_{y,atm}^d (e^{k_x d} - e^{-k_x d}). \tag{A.15}$$

From Eqs.(1.9) and (1.10),

$$\mu_0\Sigma_P\delta E_{x,atm} - \mu_0\Sigma_H\delta E_{y,atm} = \delta B_y - \delta B_{y,atm}, \tag{A.16}$$

$$\mu_0\Sigma_P\delta E_{y,atm} + \mu_0\Sigma_H\delta E_{x,atm} = -\delta B_x + \delta B_{x,atm}. \tag{A.17}$$

Thus

$$\mu_0\Sigma_P\delta E^d_{x,atm}(e^{k_xd} - e^{-k_xd}) - \mu_0\Sigma_H\delta E^d_{y,atm}(e^{k_xd} - e^{-k_xd}) = \delta E^i_x\frac{1}{V_A} - \delta E^r_x\frac{1}{V_A}, \tag{A.18}$$

$$\mu_0\Sigma_P\delta E^d_{y,atm}(e^{k_xd} - e^{-k_xd}) + \mu_0\Sigma_H\delta E^d_{x,atm}(e^{k_xd} - e^{-k_xd}) = -\delta E^r_y\frac{k_F}{\omega} - \delta E^d_{y,atm}\frac{-k_x}{i\omega}(e^{k_xd} - e^{-k_xd}). \tag{A.19}$$

Here, we define $\hat{\Sigma}_P \equiv \mu_0 V_A\Sigma_P$ and $\hat{\Sigma}_H \equiv \mu_0 V_A\Sigma_H$.

$$\delta E^i_x + \delta E^r_x = 2\delta E^d_{x,atm}\sinh(k_xd), \tag{A.20}$$

$$\delta E^r_y = 2\delta E^d_{y,atm}\sinh(k_xd), \tag{A.21}$$

$$\delta E^i_x - \delta E^r_x = 2\hat{\Sigma}_P\delta E^d_{x,atm}\sinh(k_xd) - 2\hat{\Sigma}_H\delta E^d_{y,atm}\sinh(k_xd), \tag{A.22}$$

$$-\delta E^r_y k_F - 2i\delta E^d_{y,atm}k_x\cosh(k_xd) = 2k^A_{||}\hat{\Sigma}_P\delta E^d_{y,atm}\sinh(k_xd) + 2k^A_{||}\hat{\Sigma}_H\delta E^d_{x,atm}\sinh(k_xd). \tag{A.23}$$

From these equations, we derive $\delta E_{x,is}/\delta E^i_x$ as

$$\frac{\delta E_{x,is}}{\delta E^i_x} = \frac{\delta E^i_x + \delta E^r_x}{\delta E^i_x} = \frac{2}{1 + \hat{\Sigma}_P + k^A_{||}\hat{\Sigma}^2_H/D}, \tag{A.24}$$

and $\delta B_{x,atm}/\delta B_{y,is}$ as

$$\frac{\delta B_{x,grd}}{\delta B_{y,is}} = \frac{2k_x\delta E^d_{y,atm}/i\omega}{(\delta E^i_x - \delta E^r_x)/V_A} = \frac{ik_x}{D\sinh(k_xd)}\frac{\hat{\Sigma}_H}{\hat{\Sigma}_P + k^A_{||}\hat{\Sigma}^2_H/D}, \tag{A.25}$$

where

$$D = k_F + ik_x\coth(k_xd) + k^A_{||}\hat{\Sigma}_P.$$

References

Allan, W., Transient ULF pulsations: time dependence of magnetic fields observed at the ground, *Ann. Geophys.*, **13**, 938-945, 1995.

Allan, W. and F. B. Knox, A dipole field model for axisymmetric Alfvén waves with finite ionosphere conductivities, *Planet. Space Sci.*, **27**, 79-85, 1979a.

Allan, W. and F. B. Knox, The effect of finite ionosphere conductivities on axisymmetric toroidal Alfvén wave resonances, *Planet. Space Sci.*, **27**, 939-950, 1979b.

Allan, W., E. M. Poulter and S. White, Hydromagnetic wave coupling in the magnetosphere, Plasmapause effects on impulse-excited resonance, *Planet. Space Sci.*, **34**, 1189-1200, 1986.

Buchert, S. C. and F. Budnik, Field-aligned current distributions generated by a divergent Hall current, *Geophys. Res. Lett.*, **24**, 297-300, 1997.

Chen, L. and A. Hasegawa, A theory of long-period magnetic pulsations 1. Steady state excitation of field line resonance, *J. Geophys. Res.*, **79**, 1024-1032, 1974.

Clauer, C. R. and R. L. McPherron, Mapping the local time-universal time development of magnetospheric substorms using mid-latitude magnetic observations, *J. Geophys. Res.*, **79**, 2811-2820, 1974.

Fujita, S., Modification of magnetic signals of short-period pulsations by the ionosphere, *Mem. Nat. Inst. Polar Res., Special Issue*, **36**, 287-296, 1985.

Fujita, S., K.-H. Glassmeier and K. Kamide, MHD waves generated by the Kelvin-Helmholtz instability in a nonuniform magnetosphere, *J. Geophys. Res.*, **101**, 27317-27325, 1996.

Fukushima, N., Equivalence in ground geomagnetic effect of Chapman-Vestine's and Birkeland-Alfvén's electric current-systems for polar magnetic storms, *Rep. Ionos. Space Res. Jpn.*, **23**, 219-227, 1969.

Hughes, W. J., The effect of the atmosphere and ionosphere on long period magnetospheric micropulsations, *Planet. Space Sci.*, **22**, 1157-1172, 1974.

Hughes, W. J. and D. J. Southwood, The screening of micropulsation signals by the atmosphere and ionosphere, *J. Geophys. Res.*, **81**, 3234-3240, 1976a.

Hughes, W. J. and D. J. Southwood, An illustration of modification of geomagnetic pulsation structure by the ionosphere, *J. Geophys. Res.*, **81**, 3241-3247, 1976b.

Inoue, Y. and S. Horowitz, Magneto-ionic coupling in an inhomogeneous anisotropic medium, *Radio Sci.*, **1**, 427-440, 1966a.

Inoue, Y. and S. Horowitz, Numerical solution of full-wave equation with mode coupling, *Radio Sci.*, **1**, 957-970, 1966b.

Itonaga, M., A. Yoshikawa and T.-I. Kitamura, Interaction between hydromagnetic waves and the anisotropically conducting ionosphere, *J. Geomag. Geoelectr.*, **47**, 459-474, 1995.

Jacobs, J. A., Y. Kato, S. Matsushita and V. A. Troitskaya, Classification of Geomagnetic Micropulsations, *J. Geophys. Res.*, **69**, 180-181, 1964

Kivelson, M. G., J. Etcheto and J. G. Trotignon, Global compressional oscillations of the terrestrial magnetosphere: the evidence and a model, *J. Geophys. Res.*, **89**, 9851-9856, 1984.

Maltsev, Y. P., W. B. Lyatsky and A. M. Lyatskaya, Currents over the auroral arc, *Planet. Space Sci.*, **25**, 53-57, 1977.

Mallinckrodt, A. J. and C. W. Carlson, Relations between transverse electric fields and field-aligned currents,*J. Geophys. Res.*, **83**, 1426-1432, 1978.

McHenry, M. A. and C. R. Clauer, Modeled Ground Magnetic Signatures of Flux Transfer Events, *J. Geophys. Res.*, **92**, 11231-11240, 1987.

McPherron, R. L., C. T. Russell and M. P. Aubry, Satellite studies of magnetospheric substorms on August 15, 1968, 9. Phenomenological model for substorms, *J. Geophys. Res.*, **78**, 3131-3149, 1973.

Newton, R. S., D. J. Southwood and W. J. Hughes, Damping of geomagnetic pulsations by the ionosphere, *Planet. Space Sci.*, **26**, 201-209, 1978.

Nishida, A., Ionospheric screening effect and storm sudden commencement, *J. Geophys. Res.*, **69**, 1861-1874, 1964.

Nishida, A., *Geomagnetic Diagnosis of the Magnetosphere*, Springer Verlag, New York, 1978.

Nosé, M., T. Iyemori, M. Sugiura and J. A. Slavin, A strong dawn/dusk asymmetry in Pc5 pulsation occurrence observed by the DE-1 satellite, *Geophys. Res. Lett.*, **22**, 2053-2056, 1995.

Poulter, E. M. and W. Allan, Transient ULF pulsation decay rates observed by ground based magnetometers: The contribution of spatial integration, *Planet. Space Sci.*, **33**, 607-616, 1985.

Saito, H., N. Sato, Y. Tonegawa, T. Yoshino and T. Saemundsson, Seasonal and diurnal dependence of Pc 3-5 magnetic pulsation power at geomagnetically conjugate stations in the auroral zones, *J. Geophys. Res.*, **94**, 6945-6948, 1989.

Saito, T., Long-period irregular magnetic pulsation, Pi3, *Space Sci. Rev.*, **21**, 427-467, 1978.

Samson, J. C. and G. Rostoker, Latitude-dependent characteristics of high-latitude Pc 4 and Pc 5 micropulsations, *J. Geophys. Res.*, **77**, 6133-6144, 1972.

Samson, J. C., Pi 2 pulsations: High latitude results, *Planet. Space Sci..*, **30**, 1239-1247, 1982.

Scarf, F. L., R. W. Fredericks, L. A. Frank, C. T. Russel, P. J. Coleman Jr. and M. Neugebauer, Direct correlations of large amplitude waves with suprathermal protons in the upstream solar wind, *J. Geophys. Res.*, **75**, 7316-7322, 1970.

Scholer, M, On the motion of artificial ion clouds in the magnetosphere, *Planet. Space Sci.*, **18**, 977-1004, 1970.

Southwood, D. J., Some features of field line resonances in the magnetosphere, *Planet. Space Sci.*, **22**, 483-491, 1974.

Takahashi, K., S. Ohtani and K. Yumoto, AMPTE CCE observations of Pi 2 pulsations

in the inner magnetosphere, *Geophys. Res. Lett..*, **19**, 1447-1450, 1992.

Tamao, T., The structure of three-dimensional hydromagnetic waves in a uniform cold plasma, *J. Geomag. Geoelectr.*, **16**, 89-114, 1964.

Tamao, T., Transmission and coupling resonance hydromagnetic disturbances in the non-uniform Earth's magnetosphere, *Sci. Rep. Tohoku Univ. Ser. 5*, **17** 43-72, 1965.

Tamao, T., Magnetosphere-ionosphere interaction through hydromagnetic waves, *Proc. Conf. Achievements of the IMS, 26-28 June 1984, Graz, Austria, ESA SP-217*, 427-435, 1984.

Tamao, T., Direct contribution of oblique field-aligned currents to ground magnetic fields, *J. Geophys. Res.*, **91**, 183-189, 1986.

Wright, A. N., Dispersion and wave coupling in inhomogeneous MHD waveguides, *J. Geophys. Res.*, **99**, 159-167, 1994.

Yoshikawa, A. and M. Itonaga, Reflection of shear Alfvén waves at the ionosphere and the divergent Hall current, *Geophys. Res. Lett.*, **23**, 101-104, 1996.

Yoshikawa, A. M. Itonaga, and T. Kitamura, Effect of the ionospheric induction current on magnetohydrodynamic waves in the magnetosphere, *Proc. NIPR Symp. Upper Atmos. Phys.*, **8**, 49-59, 1995.

Yumoto, K., Evidences of magnetospheric cavity Pi2 waves, *J. Geomag. Geoelectr.*, **42**, 1281-1290, 1990.

Yumoto, K., A. Isono, K. Shiokawa, H. Matsuoka, Y. Tanaka, F. W. Menk, B. J. Fraser and 210° Magnetic Meridian Magnetic Observation Group, Global cavity mode-like and localized field-line Pc3-4 oscillations stimulated by interplanetary impulses (Si/Sc): Initial results from the 210° MM magnetic observations, *Solar Wind Sources of Magnetospheric Ultra-Low-Frequency Waves, Geophys. Monogr.*, vol.81, edited by M. J. Engebretson, K. Takahashi and M. Scholer, AGU, Washington, D.C., pp.335-344, 1994.

Yumoto, K., Y. Tanaka, T. Oguti, K. Shiokawa, Y. Yoshimura, A. Isono, B. J. Fraser, F. W. Menk, J. W. Lynn, M. Seto and 210° MM Magnetic Observation Group, Globally

coordinated magnetic observations along 210° magnetic meridian during STEP period: 1. Preliminary results of low-latitude Pc3's, *J. Geomag. Geoelectr.*, **44**, 261-276, 1992.

Zhang, X., R. H. Comfort, Z. E. Musielak, T. E. Moore, D. L. Gallagher and J. L. Green, Propagation characteristics of Pc 3 compressional waves generated at the dayside magnetopause, *J. Geophys. Res.*, **98**, 15403-15410, 1993.

Ziesolleck, C. W. S., B. J. Fraser, F. W. Menk and P. W. McNabb, Spatial characteristics of low-latitude Pc3-4 geomagnetic pulsations, *J. Geophys. Res.*, **98**, 197-207, 1993.

Tables

		March				June			
L		Φ=0°	Φ=90°	Φ=180°	Φ=270°	Φ=0°	Φ=90°	Φ=180°	Φ=270°
6.0	(S)	11.58	9.99	11.51	12.62	15.12	10.30	11.18	12.10
	(N)	11.94	13.53	12.01	10.90	8.40	13.21	12.34	11.42
	(N/S)	1.03	1.35	1.04	0.86	0.56	1.28	1.10	0.94
4.0	(S)	7.46	6.24	7.65	8.66	8.85	6.43	7.12	7.64
	(N)	8.07	9.29	7.88	6.87	6.68	9.10	8.41	7.89
	(N/S)	1.08	1.49	1.03	0.79	0.76	1.41	1.18	1.03
2.0	(S)	3.33	2.84	3.63	4.49	3.25	3.00	3.43	3.84
	(N)	4.25	4.74	3.95	3.09	4.33	4.58	4.15	3.74
	(N/S)	1.27	1.67	1.09	0.69	1.33	1.53	1.21	0.97
		September				December			
L		Φ=0°	Φ=90°	Φ=180°	Φ=270°	Φ=0°	Φ=90°	Φ=180°	Φ=270°
6.0	(S)	10.52	9.01	11.09	12.01	12.61	10.76	9.79	12.89
	(N)	12.99	14.50	12.43	11.51	10.90	12.76	13.73	10.63
	(N/S)	1.23	1.61	1.12	0.96	0.86	1.19	1.40	0.83
4.0	(S)	6.55	5.60	7.14	8.12	8.06	6.90	6.88	8.76
	(N)	8.98	9.93	8.39	7.41	7.47	8.63	8.65	6.77
	(N/S)	1.37	1.77	1.18	0.91	0.93	1.25	1.26	0.77
2.0	(S)	3.08	2.59	3.29	4.25	3.18	2.95	3.67	4.24
	(N)	4.50	4.98	4.29	3.32	4.40	4.63	3.91	3.33
	(N/S)	1.46	1.92	1.30	0.78	1.38	1.57	1.06	0.79

Table 4.1: The Alfvén speed in the ionosphere ($V_{A,is}$).

L		Φ=0°	Φ=90°	Φ=180°	Φ=270°
6.0	(S)	0.44	0.51	0.15	0.16
	(N)	0.21	0.27	0.06	0.21
	(N/S)	0.47	0.52	0.38	1.34
4.0	(S)	0.53	0.55	0.19	0.23
	(N)	0.28	0.33	0.10	0.30
	(N/S)	0.53	0.60	0.54	1.32
2.0	(S)	0.80	0.53	0.37	0.44
	(N)	0.50	0.57	0.28	0.56
	(N/S)	0.63	1.08	0.76	1.25

Table 4.2: The values of z_0 derived from the magnetic inclination ($z_0 = 1/\tan I$).

L	Freq.(mHz)	Reference
6	6.0	Samson and Rostoker [1972]
4	10.7	Samson and Rostoker [1972]
2	27.5	Ziesolleck *et al.* [1993]

Table 4.3: The eigenfrequencies of the standing Alfvén oscillation in each L-shells.

Mar.		Φ=0°			Φ=90°			Φ=180°			Φ=270°		
L		$\bar{\Sigma}_{P0}$	$\bar{\Sigma}_{H0}$	$\bar{\Sigma}_{H0}/\bar{\Sigma}_{P0}$	$\bar{\Sigma}_{P0}$	$\bar{\Sigma}_{H0}$	$\bar{\Sigma}_{H0}/\bar{\Sigma}_{P0}$	$\bar{\Sigma}_{P0}$	$\bar{\Sigma}_{H0}$	$\bar{\Sigma}_{H0}/\bar{\Sigma}_{P0}$	$\bar{\Sigma}_{P0}$	$\bar{\Sigma}_{H0}$	$\bar{\Sigma}_{H0}/\bar{\Sigma}_{P0}$
6.0	(S)	6.48	9.76	1.51	12.82	20.18	1.57	8.52	14.61	1.72	7.51	11.59	1.54
	(N)	10.33	17.23	1.67	10.88	17.32	1.59	6.07	9.16	1.51	9.00	14.78	1.64
	(N/S)	1.59	1.76	1.11	0.85	0.86	1.01	0.71	0.63	0.88	1.20	1.28	1.07
4.0	(S)	7.66	11.22	1.46	14.10	21.68	1.54	7.54	13.05	1.73	7.02	11.06	1.58
	(N)	9.01	15.21	1.69	9.95	16.21	1.63	5.94	8.82	1.48	8.29	13.95	1.68
	(N/S)	1.18	1.36	1.15	0.71	0.75	1.06	0.79	0.68	0.86	1.18	1.26	1.07
2.0	(S)	17.96	26.99	1.50	25.01	40.39	1.61	10.66	18.72	1.76	10.92	18.19	1.67
	(N)	12.69	22.04	1.74	14.30	24.63	1.72	9.47	14.57	1.54	14.54	23.47	1.61
	(N/S)	0.71	0.82	1.16	0.57	0.61	1.07	0.89	0.78	0.88	1.33	1.29	0.97
Jun.		Φ=0°			Φ=90°			Φ=180°			Φ=270°		
L		$\bar{\Sigma}_{P0}$	$\bar{\Sigma}_{H0}$	$\bar{\Sigma}_{H0}/\bar{\Sigma}_{P0}$	$\bar{\Sigma}_{P0}$	$\bar{\Sigma}_{H0}$	$\bar{\Sigma}_{H0}/\bar{\Sigma}_{P0}$	$\bar{\Sigma}_{P0}$	$\bar{\Sigma}_{H0}$	$\bar{\Sigma}_{H0}/\bar{\Sigma}_{P0}$	$\bar{\Sigma}_{P0}$	$\bar{\Sigma}_{H0}$	$\bar{\Sigma}_{H0}/\bar{\Sigma}_{P0}$
6.0	(S)	0.16	0.49	3.14	4.23	6.94	1.64	4.85	8.06	1.66	2.36	4.04	1.71
	(N)	13.10	20.99	1.60	14.22	23.30	1.64	9.33	15.62	1.67	12.23	19.90	1.63
	(N/S)	84.42	43.05	0.51	3.36	3.36	1.00	1.92	1.94	1.01	5.18	4.93	0.95
4.0	(S)	0.49	1.32	2.69	6.49	10.49	1.61	5.14	8.27	1.61	3.41	5.48	1.60
	(N)	11.07	17.71	1.60	12.40	20.33	1.64	8.06	13.42	1.66	10.85	17.53	1.62
	(N/S)	22.45	13.37	0.60	1.91	1.94	1.02	1.57	1.62	1.03	3.18	3.20	1.01
2.0	(S)	12.20	15.02	1.23	17.37	27.71	1.60	9.25	15.08	1.63	8.80	12.67	1.44
	(N)	14.18	23.67	1.67	16.58	27.70	1.67	10.61	17.60	1.66	15.14	25.95	1.71
	(N/S)	1.16	1.58	1.36	0.95	1.00	1.05	1.15	1.17	1.02	1.72	2.05	1.19

Table 4.4: The normalized Pedersen and Hall conductivities and ratios of the conductivities.

Sep.		Φ=0°			Φ=90°			Φ=180°			Φ=270°		
L		$\bar{\Sigma}_{P0}$	$\bar{\Sigma}_{H0}$	$\bar{\Sigma}_{H0}/\bar{\Sigma}_{P0}$	$\bar{\Sigma}_{P0}$	$\bar{\Sigma}_{H0}$	$\bar{\Sigma}_{H0}/\bar{\Sigma}_{P0}$	$\bar{\Sigma}_{P0}$	$\bar{\Sigma}_{H0}$	$\bar{\Sigma}_{H0}/\bar{\Sigma}_{P0}$	$\bar{\Sigma}_{P0}$	$\bar{\Sigma}_{H0}$	$\bar{\Sigma}_{H0}/\bar{\Sigma}_{P0}$
6.0	(S)	7.68	10.90	1.42	15.13	21.76	1.44	8.89	15.08	1.70	7.92	12.19	1.54
	(N)	10.06	16.63	1.65	10.89	16.48	1.51	5.54	8.44	1.52	8.43	13.85	1.64
	(N/S)	1.31	1.53	1.16	0.72	0.76	1.05	0.62	0.56	0.90	1.06	1.14	1.07
4.0	(S)	8.65	12.07	1.40	15.42	22.74	1.47	7.76	13.34	1.72	7.30	11.59	1.59
	(N)	8.87	14.84	1.67	10.07	15.68	1.56	5.12	8.26	1.61	7.89	13.33	1.69
	(N/S)	1.03	1.23	1.20	0.65	0.69	1.06	0.66	0.62	0.94	1.08	1.15	1.06
2.0	(S)	19.66	28.39	1.44	26.32	41.42	1.57	10.89	18.95	1.74	10.94	18.58	1.70
	(N)	12.63	21.75	1.72	14.41	24.22	1.68	8.42	13.96	1.66	12.86	22.61	1.76
	(N/S)	0.64	0.77	1.19	0.55	0.58	1.07	0.77	0.74	0.95	1.18	1.22	1.04

Dec.		Φ=0°			Φ=90°			Φ=180°			Φ=270°		
L		$\bar{\Sigma}_{P0}$	$\bar{\Sigma}_{H0}$	$\bar{\Sigma}_{H0}/\bar{\Sigma}_{P0}$	$\bar{\Sigma}_{P0}$	$\bar{\Sigma}_{H0}$	$\bar{\Sigma}_{H0}/\bar{\Sigma}_{P0}$	$\bar{\Sigma}_{P0}$	$\bar{\Sigma}_{H0}$	$\bar{\Sigma}_{H0}/\bar{\Sigma}_{P0}$	$\bar{\Sigma}_{P0}$	$\bar{\Sigma}_{H0}$	$\bar{\Sigma}_{H0}/\bar{\Sigma}_{P0}$
6.0	(S)	11.25	19.02	1.69	16.74	29.08	1.74	10.85	18.61	1.71	10.13	16.84	1.66
	(N)	5.79	9.05	1.56	3.73	5.53	1.48	0.12	0.41	3.47	2.86	4.71	1.64
	(N/S)	0.51	0.48	0.92	0.22	0.19	0.85	0.01	0.02	2.02	0.28	0.28	0.99
4.0	(S)	10.78	18.48	1.71	16.00	28.07	1.75	9.11	15.67	1.72	8.93	14.71	1.65
	(N)	6.26	9.35	1.49	5.38	7.60	1.41	0.34	0.99	2.90	4.30	6.49	1.51
	(N/S)	0.58	0.51	0.87	0.34	0.27	0.81	0.04	0.06	1.69	0.48	0.44	0.92
2.0	(S)	19.03	33.65	1.77	25.28	45.45	1.80	11.71	20.43	1.74	12.69	21.04	1.66
	(N)	11.03	17.48	1.58	11.41	16.77	1.47	4.94	7.47	1.51	10.96	15.75	1.44
	(N/S)	0.58	0.52	0.90	0.45	0.37	0.82	0.42	0.37	0.87	0.86	0.75	0.87

Table 4.4: (continued)

Station	Geographic		Geomagnetic		L
	Lat.	Lon.	Lat.	Lon.	
Kotzebue (KOT)	66.88	197.40	64.63	249.25	5.45
Macquarie Isl. (MCQ)	-54.50	158.95	-64.77	247.60	5.50
Moshiri (MSR)	44.37	142.27	37.76	212.96	1.60
Birdsville (BRV)	-25.54	139.21	-37.30	212.86	1.57

Table 4.5: Geographic and corrected geomagnetic coordinates of stations in 210° MM chain [Yumoto *et al.*, 1992]. Geomagnetic coordinates and L-values are calculated with IGRF85 model for 100km altitude of each station on January 1, 1991.

	High Latitude (KOT and MCQ)	Low Latitude (MSR and BRV)
Pc 3	winter > summer	MSR > BRV
Pc 4-5	KOT > MCQ	—

Table 4.6: North-south power ratios of Pc pulsations observed in the 210° MM chain after Yumoto [private communication].

Station pair	$\sin I$	season (north)	Σ_H	Σ_H/Σ_P	V_A
KOT/MCQ	0.991	summer	1.97	0.98	0.87
		winter	0.33	1.07	0.99
MSR/BRV	1.01	summer	1.24	1.00	0.93
		winter	0.70	0.91	1.04

Table 4.7: Seasonal variations of ratios of the parameters (the inclination, the ionospheric conductivity and the Alfvén speed) in 210°stations.

Station	Geographic		Geomagnetic		L
	Lat.	Lon.	Lat.	Lon.	
Syowa station (SYO)	-69.00	39.58	-66.22	71.44	6.15
Husafell (HUS)	64.67	-21.03	65.87	69.36	5.99
Tjörnes (TJO)	66.20	-17.12	66.80	73.76	6.45

Table 4.8: Geographic and corrected geomagnetic coordinates of Syowa and Iceland conjugate stations [Saito *et al.*, 1989].

Station pair	$\sin I$	season (north)	Σ_H	Σ_H/Σ_P	V_A
HUS/SYO	1.08	Summer	11.701	0.688	0.759
		Winter	0.244	0.996	1.479
TJO/SYO	1.08	Summer	11.552	0.693	0.754
		Winter	0.217	1.027	1.515

Table 4.9: Ratios of the parameters (the ionospheric conductivity and the Alfvén speed) between Syowa-Iceland stations in solstice seasons.

Figures

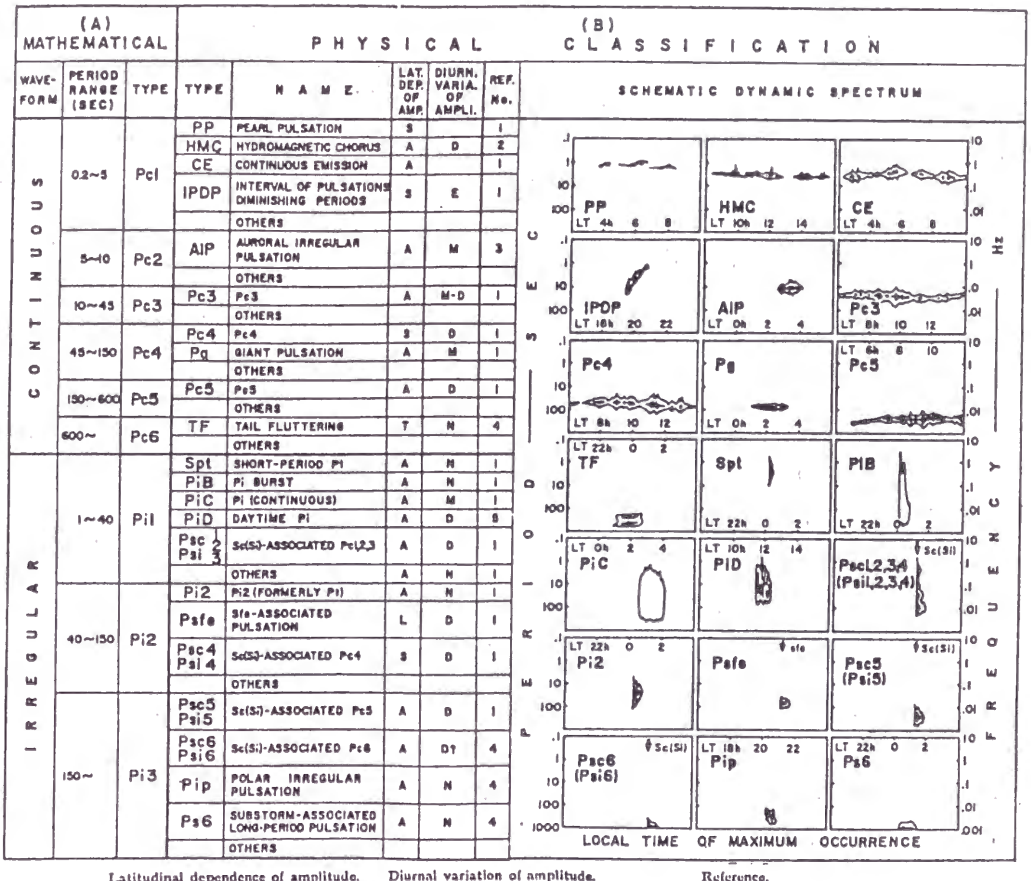

Figure 1.1: Classification and the features of the geomagnetic pulsations. [Saito, 1978]

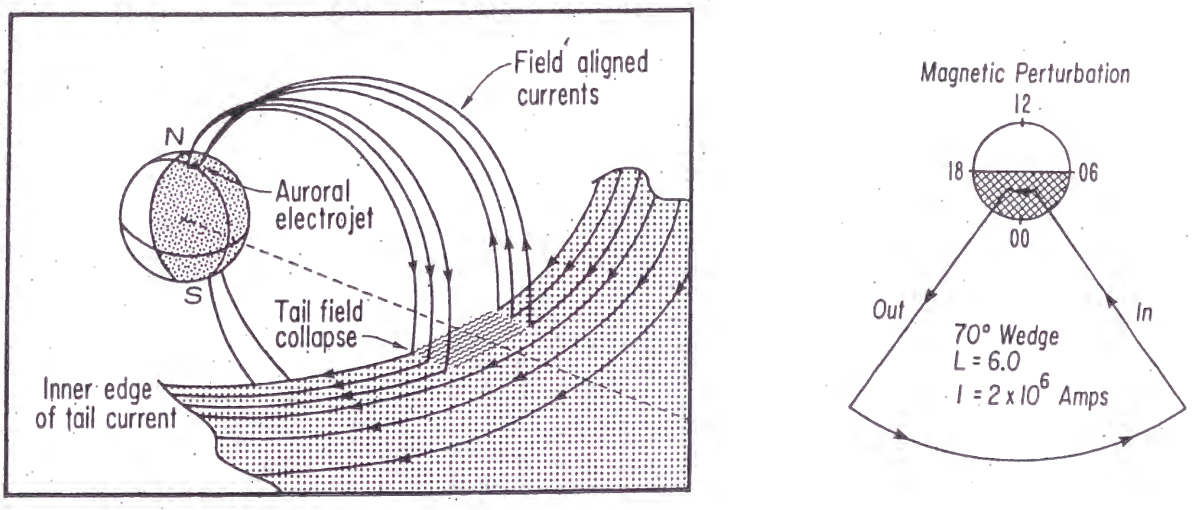

Figure 1.2: (Left) A schematic figure of the current disruption. The cross tail current is disrupted in the collapse and the field aligned currents flow into and out of the ionosphere. (Right) The current wedge viewed from north. FAC and ionospheric current and the tail current compose a closed circuit. [McPherron *et al.*, 1973]

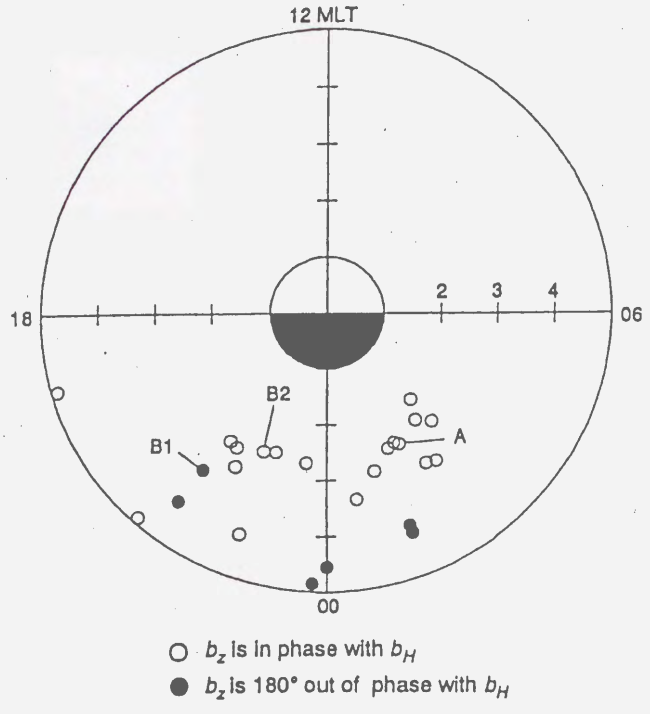

Figure 1.3: The locations of AMPTE CCE satellite at the onset of Pi 2 events. Pi 2 pulsation in the magnetosphere is mainly observed in the nightside. [Takahashi *et al.*, 1992]

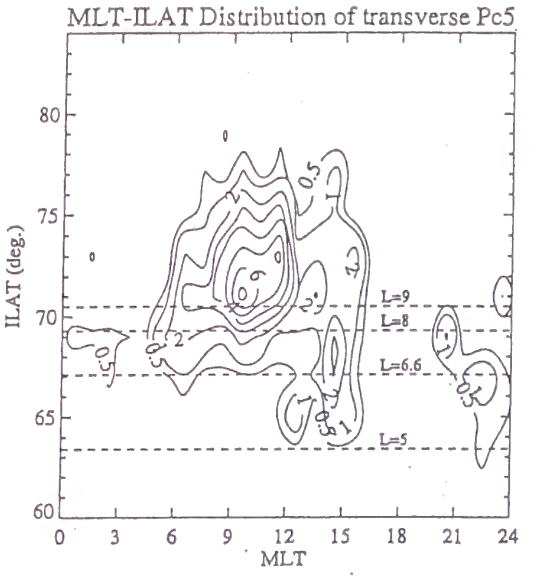

Figure 1.4: The contour plot of occurence of Pc 5 pulsations [Nose *et al.*, 1995]

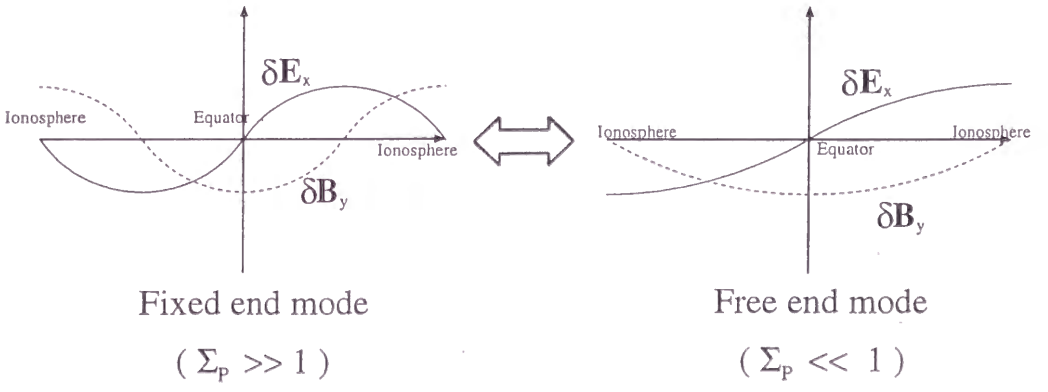

Figure 1.5: A schematic illustration of the modal structure of the standing Alfvén oscillation. (Left) When the Pedersen conductivity is zero, the electric field of the standing Alfvén oscillation has an anti-node and the magnetic field has a node in the ionosphere. (Right) When the Pedersen conductivity becomes larger, the relation is reverse.

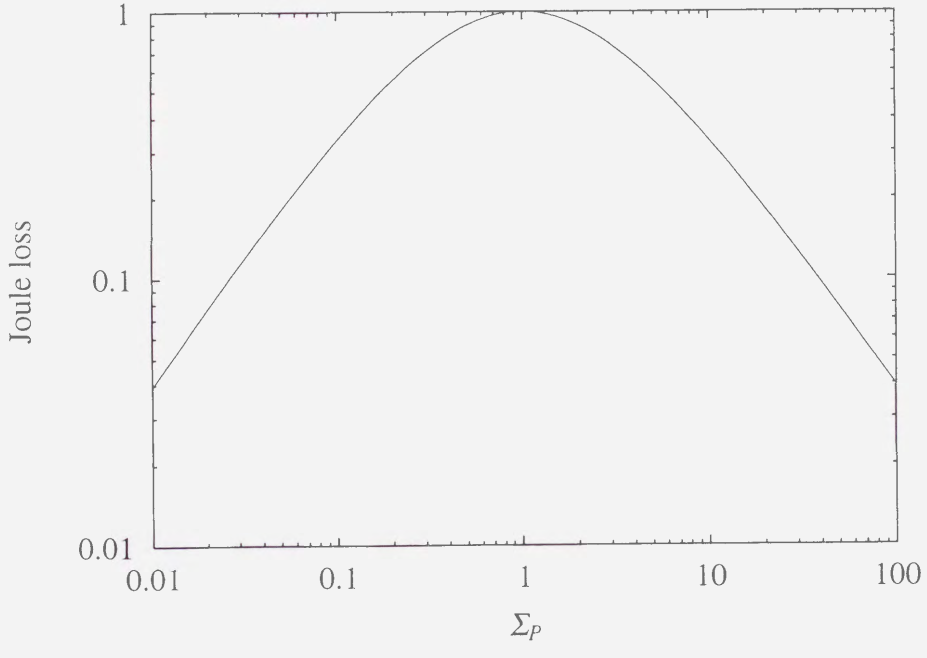

Figure 1.6: The Joule loss of the standing Alfvén oscillation shown in Eq. (1.7) versus the Pedersen conductivity. $\Sigma_A = 1$.

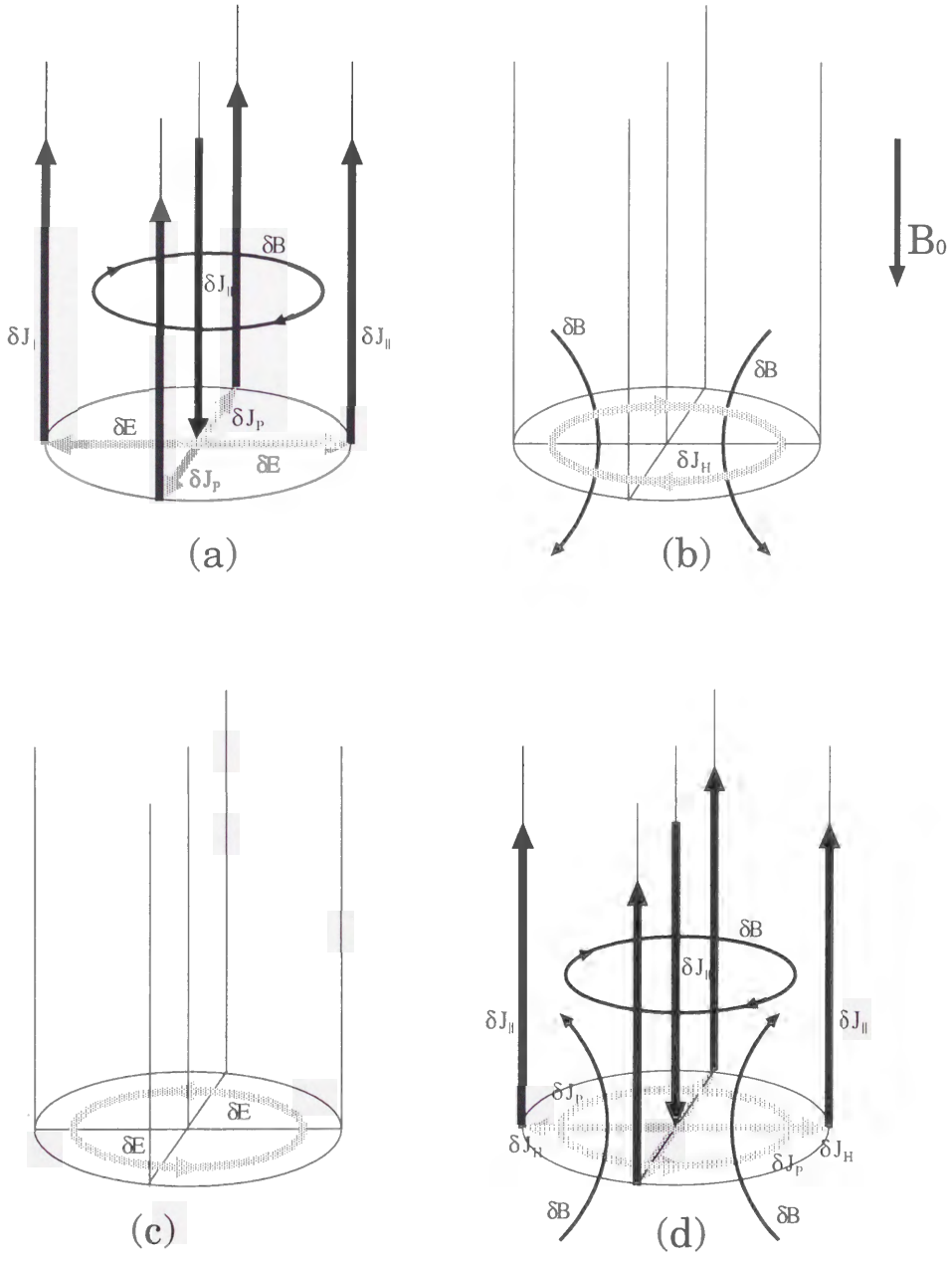

Figure 1.7: Schematic illustrations for electromagnetic field and current associated with the Alfvén wave incidence. (a) When the Alfvén wave impinges on the ionosphere, the Pedersen current closes FAC associated with Alfvén wave. (b) The primary electric field induces the Hall current and the magnetic disturbance. (c) The secondary electric field is induced by the Hall current. (d) This electric field again induces the Pedersen and Hall current.

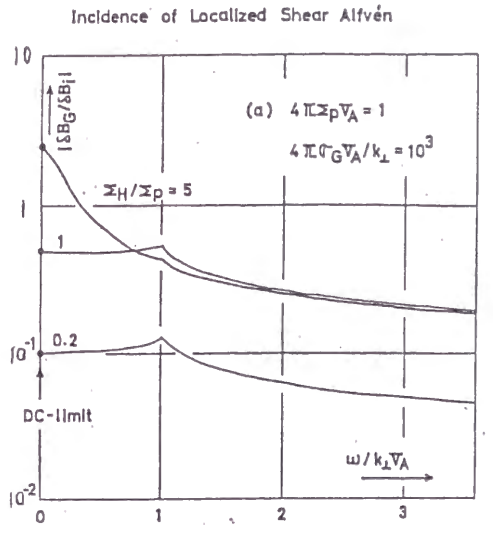

Figure 1.8: The ratio of the ground magnetic perturbation to the magnetic perturbation above the ionosphere as a function of $\omega/k_\perp V_A$ when the Alfvén wave impinges on the ionosphere. The case of $\Sigma_H/\Sigma_P = 0.2$, 1 and 5 are plotted [Tamao, 1984]

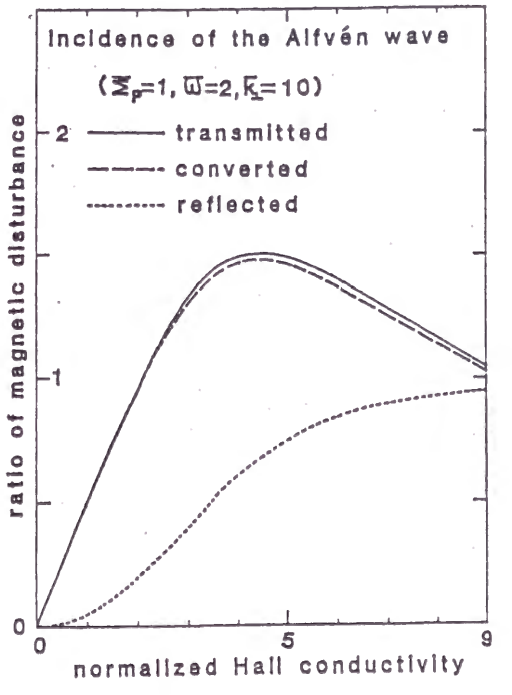

Figure 1.9: The intensity of the ground magnetic perturbation (solid line), that of the converted fast wave (dashed line) and that of reflected Alfvén wave (dotted line) normalized by the incident Alfvén wave intensity as a function of Σ_H. [Fujita, 1985]

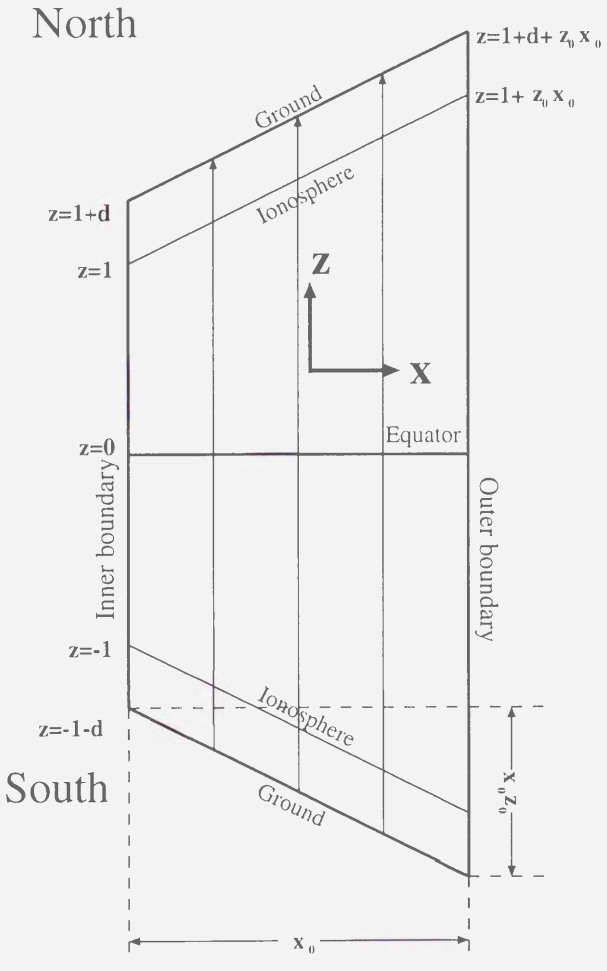

Figure 2.1: The schematic figure of the model used in the present study. The inner and outer boundaries are located at $x = 0$ and x_0. The ionospheres at $x = 0$ are located at $z = \pm 1$ ($\pm$ refer to the ionosphere in the northern and southern hemispheres, respectively) and that at $x = x_0$ is $z = \pm(1 + z_0 x_0)$. The distance between the ionosphere and the Earth is d. The z coordinate of the magnetic equator is $z = 0$.

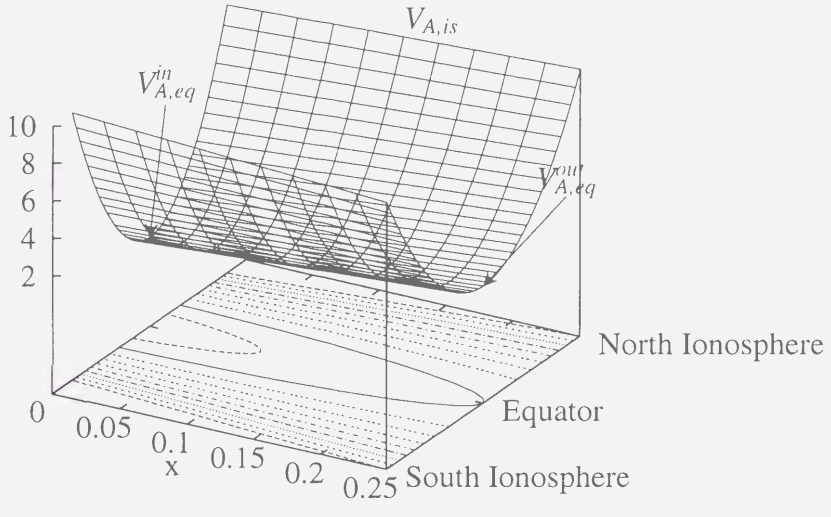

Figure 2.2: The profile and contour plot of the Alfvén speed used in the present study. $V_{A,is}$ is constant in each ionosphere regardless of the x coordinate.

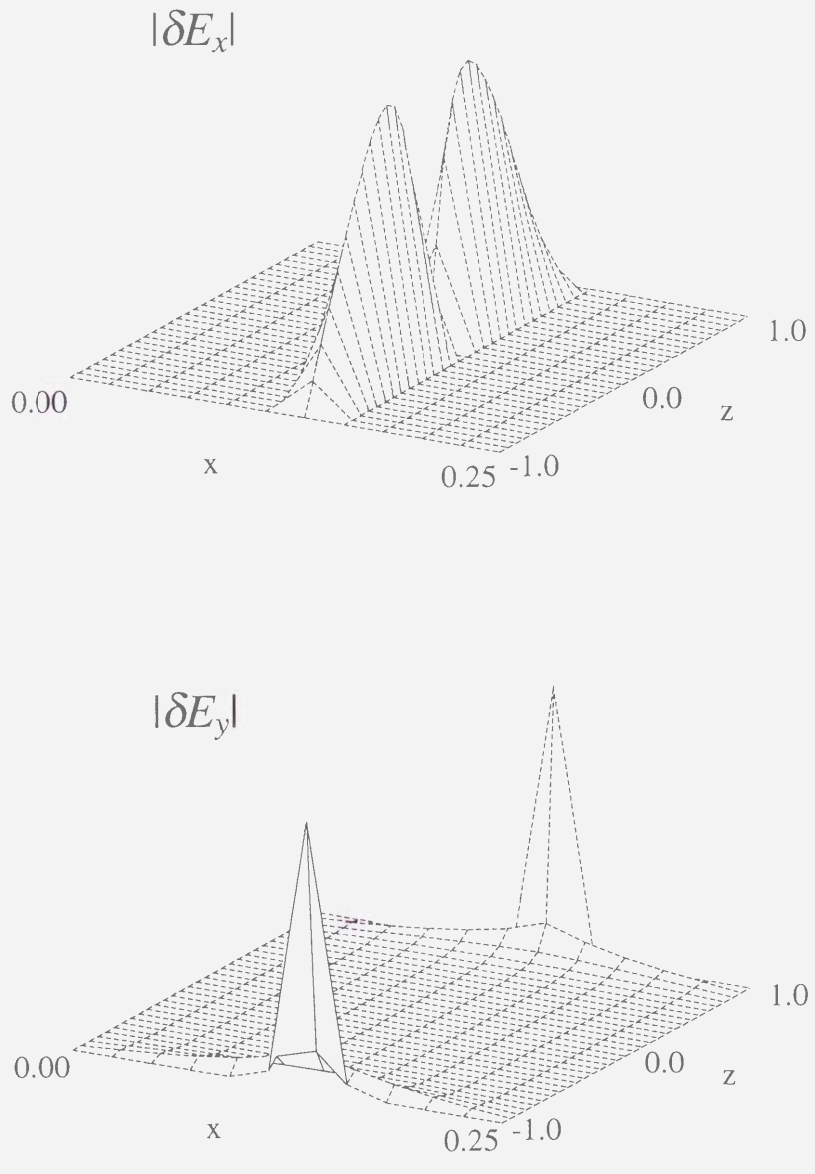

Figure 2.3: The 2D profiles of the electric field intensity associated with the standing Alfvén oscillation ($|\delta E_x|$) and that of the fast mode wave induced through the ionospheric Hall current ($|\delta E_y|$). Parameters are $\bar{\Sigma}_{P0}$= $\bar{\Sigma}_{H0}$= 100, $z_0 = 0$ and $V_{A,is} = 10$. Note that the main magnetic field is vertical to the ionosphere ($z_0 = 0$).

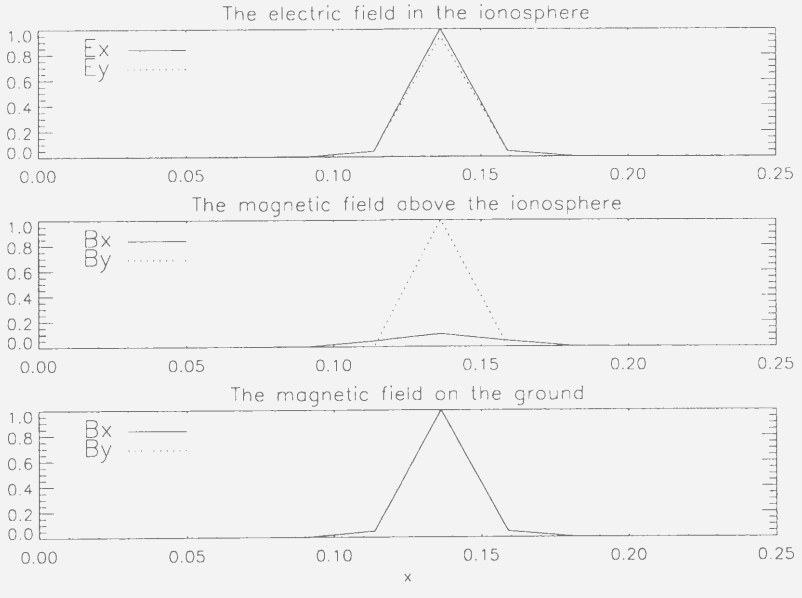

Figure 2.4: Latitudinal (x-direction) intensity profiles of the electric field perturbations in the ionosphere (top), those of the magnetic field perturbations just above the ionosphere (middle) and those on the ground (bottom). The parameters are same as that used in Fig. 2.3. The x and y components are represented with the solid and dotted lines respectively.

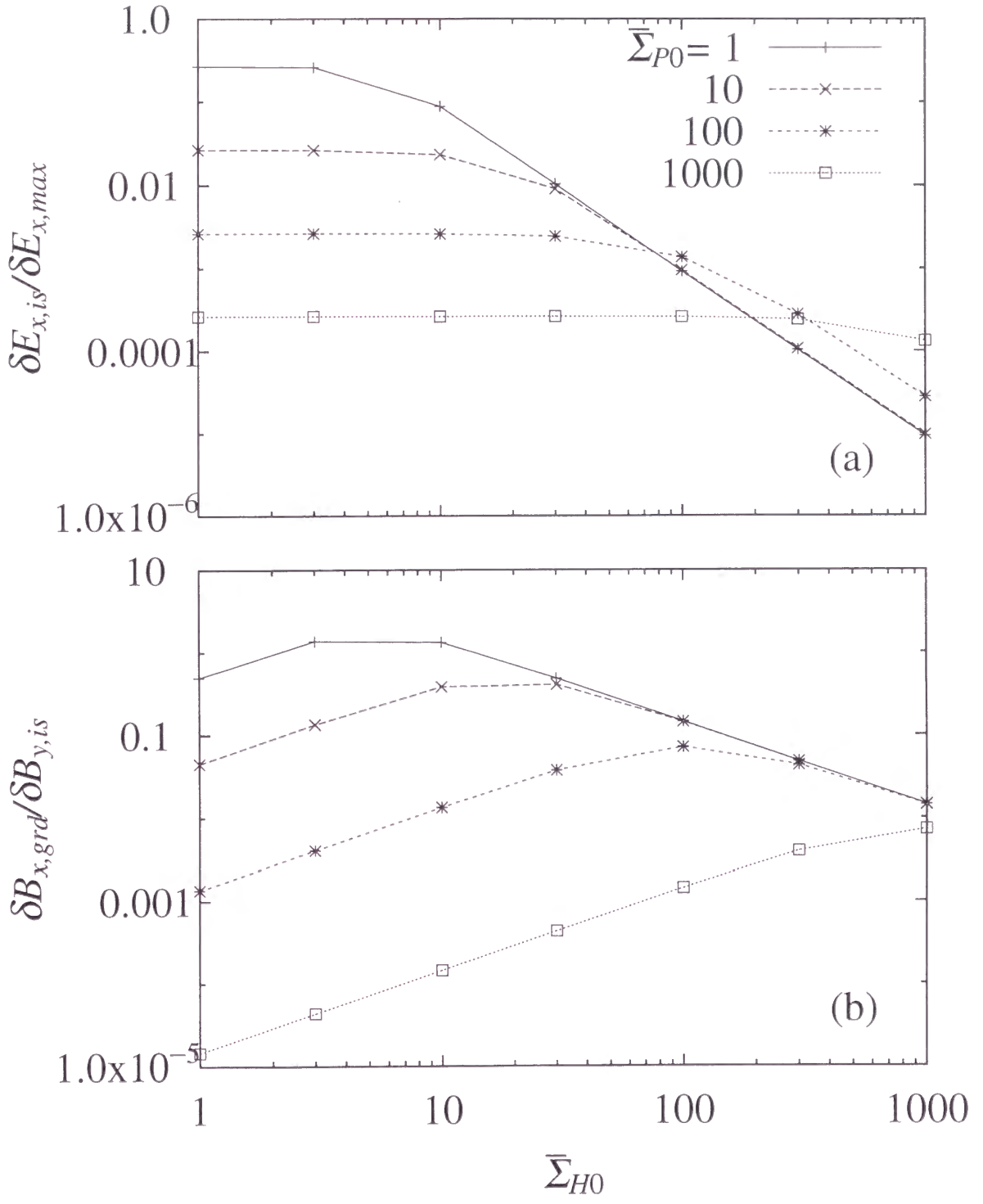

Figure 3.1: (a) $\delta E_{x,is}/\delta E_{x,max}$ and (b) $\delta B_{x,grd}/\delta B_{y,is}$ of the second mode standing Alfvén oscillation as functions of $\bar{\Sigma}_{H0}$. The ratios in 4 cases of $\bar{\Sigma}_{P0}$ (1, 10, 100 and 1000) are shown.

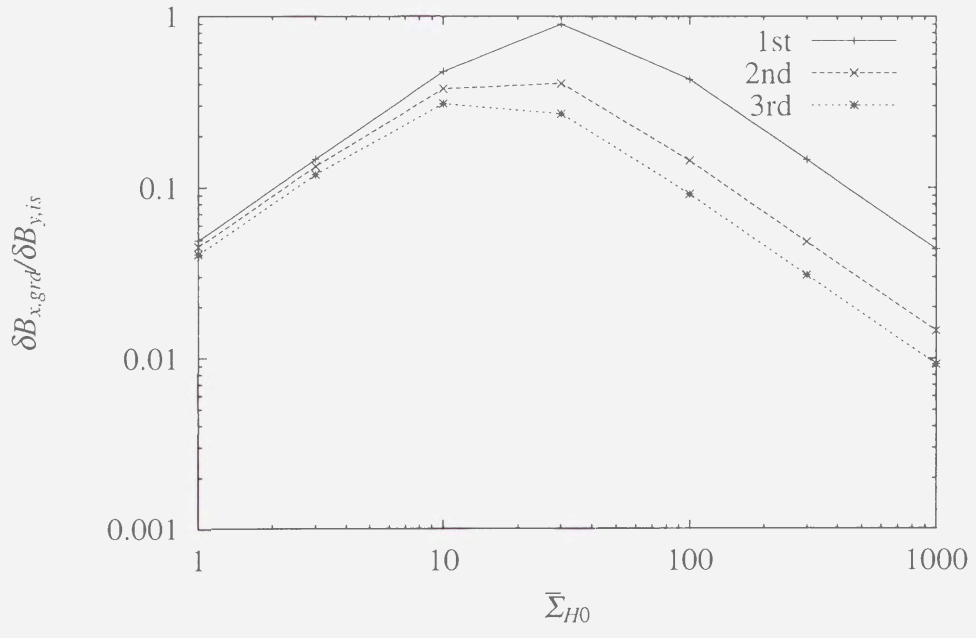

Figure 3.2: $\delta B_{x,grd}/\delta B_{y,is}$ of the first three harmonics of the standing Alfvén oscillation are plotted as functions of $\bar{\Sigma}_{H0}$ where $\bar{\Sigma}_{P0} = 10$. The solid, dashed and dotted lines represent the fundamental, second, and third harmonic modes respectively.

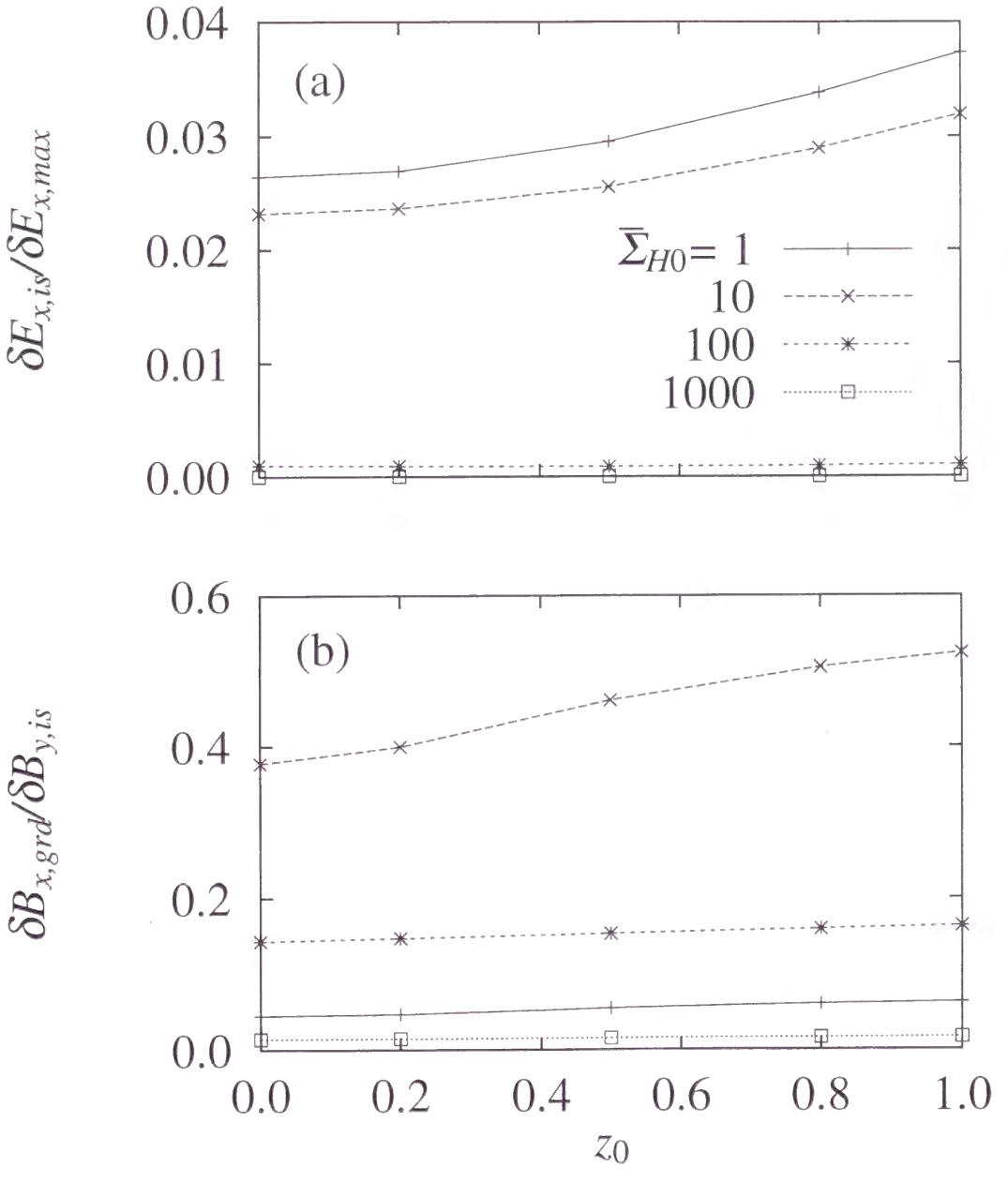

Figure 3.3: (a) $\delta E_{x,is}/\delta E_{x,max}$ and (b) $\delta B_{x,grd}/\delta B_{y,is}$ as functions of z_0. The ratios in 4 cases of $\bar{\Sigma}_{H0}/\bar{\Sigma}_{P0}$ (0.1, 1, 10 and 100) are shown ($\bar{\Sigma}_{P0} = 10$).

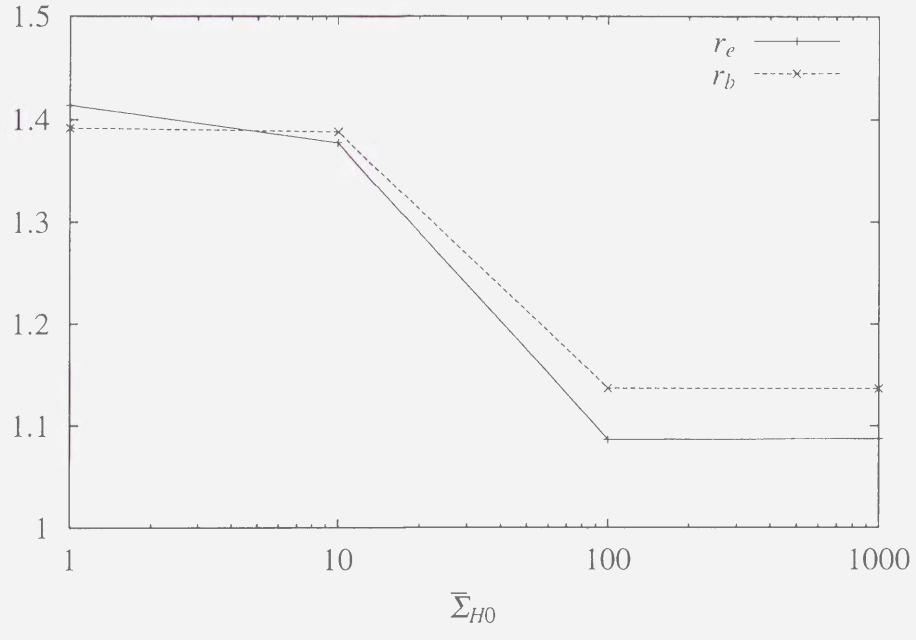

Figure 3.4: r_e (defined in Eq.(3.5)) and r_b (Eq.(3.6)) as functions of $\bar{\Sigma}_{H0}$. The solid and dashed lines are r_e and r_b, respectively.

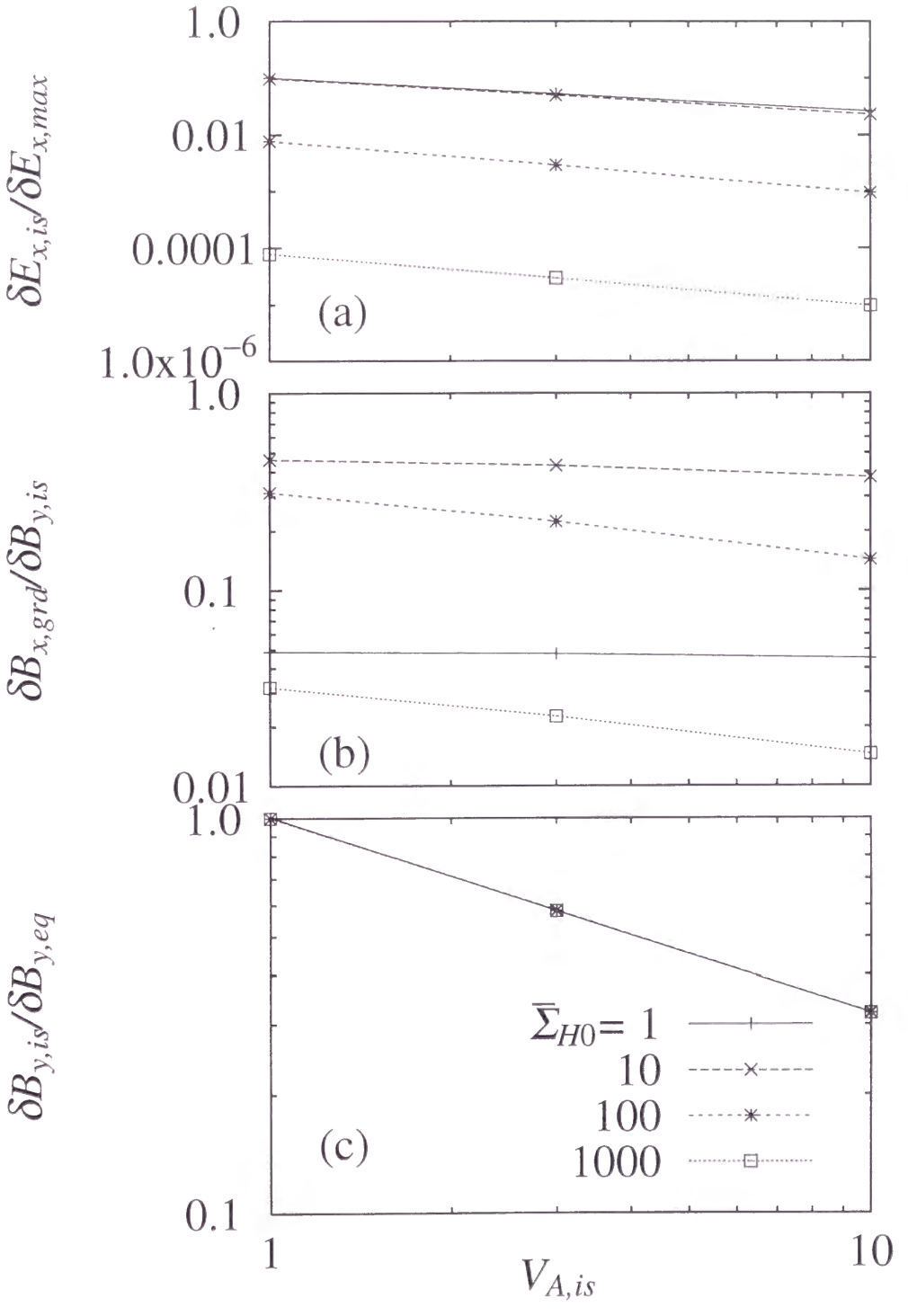

Figure 3.5: (a) $\delta E_{x,is}/\delta E_{x,max}$, (b) $\delta B_{x,grd}/\delta B_{y,is}$, and (c) $\delta B_{y,is}/\delta B_{y,eq}$ as functions of $V_{A,is}$. The values of the conductivities are as same as those of Fig.3.3.

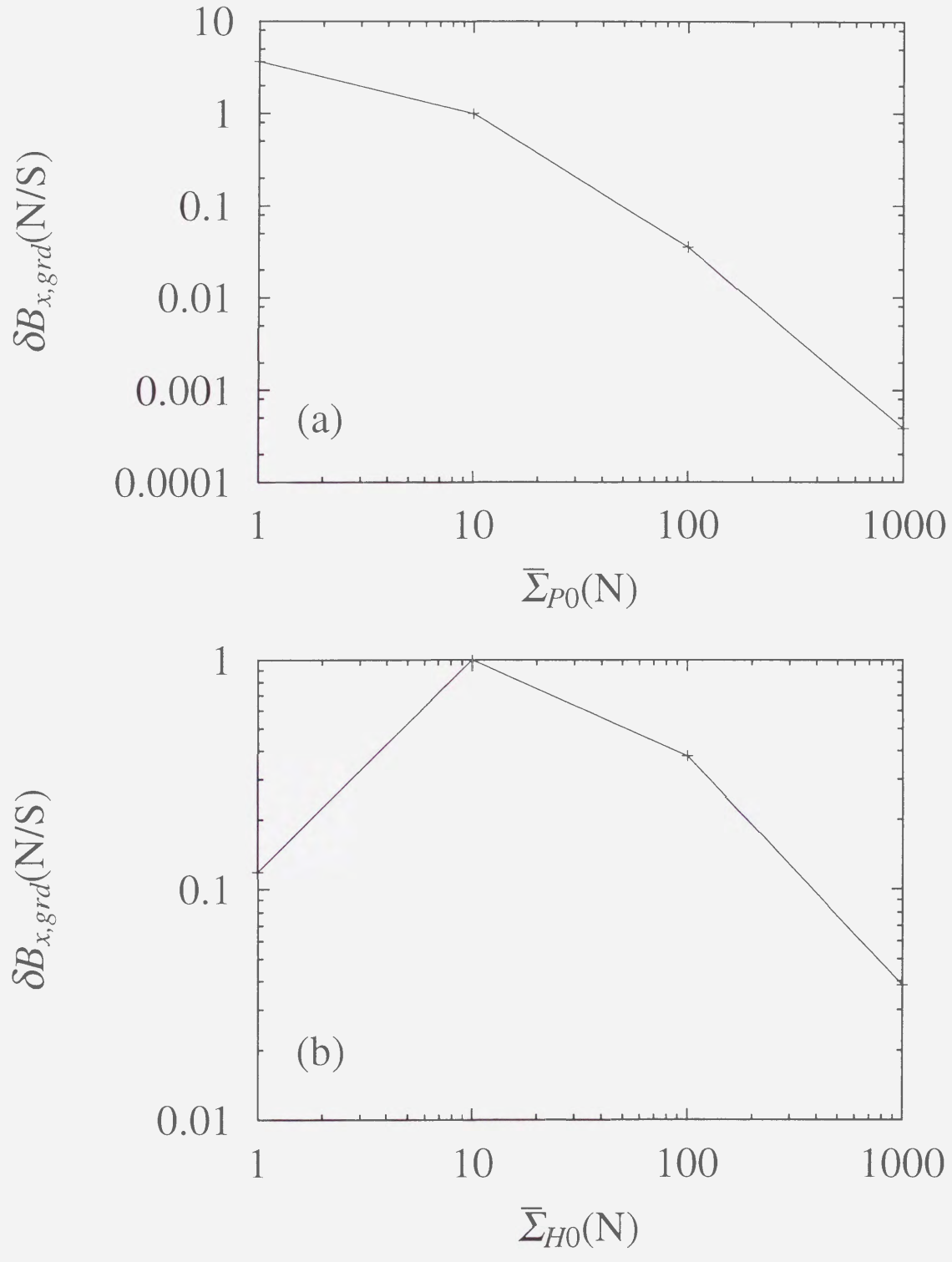

Figure 3.6: (a) $\delta B_{x,grd}$(N/S) as a function of $\bar{\Sigma}_{P0}$(N). $\bar{\Sigma}_{P0}$(S) = $\bar{\Sigma}_{H0}$(N,S) = 10. (b) $\delta B_{x,grd}$(N/S) as a function of $\bar{\Sigma}_{H0}$(N). $\bar{\Sigma}_{P0}$(N,S) = $\bar{\Sigma}_{H0}$(S) = 10. In both panels, $z_0 = 0$ and $V_{A,is} = 10$ in both hemispheres.

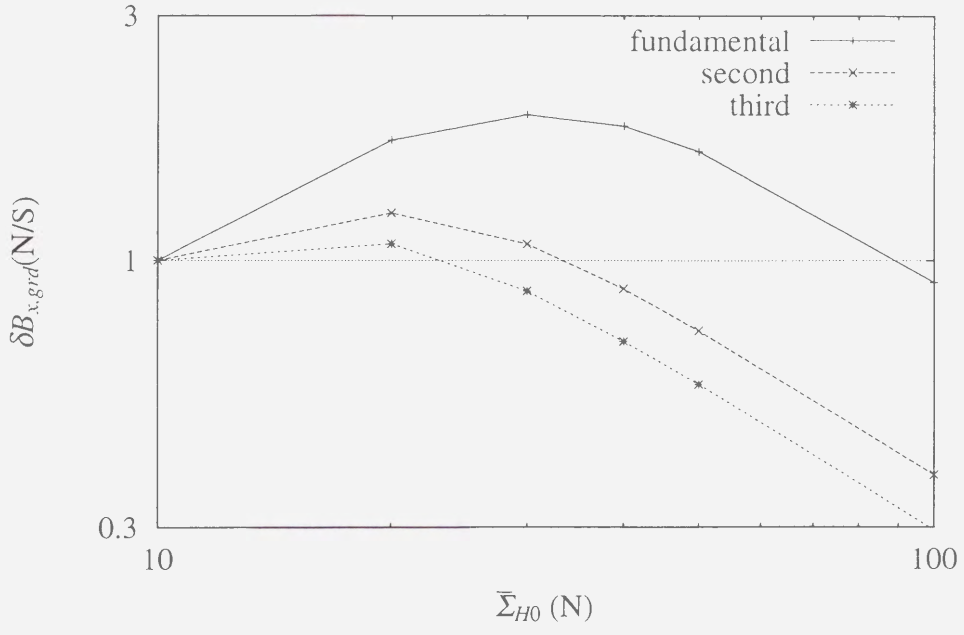

Figure 3.7: $\delta B_{x,grd}$(N/S) of the first three harmonics of the standing Alfvén oscillation. The conductivities are as same as those used for Fig.3.6(b).

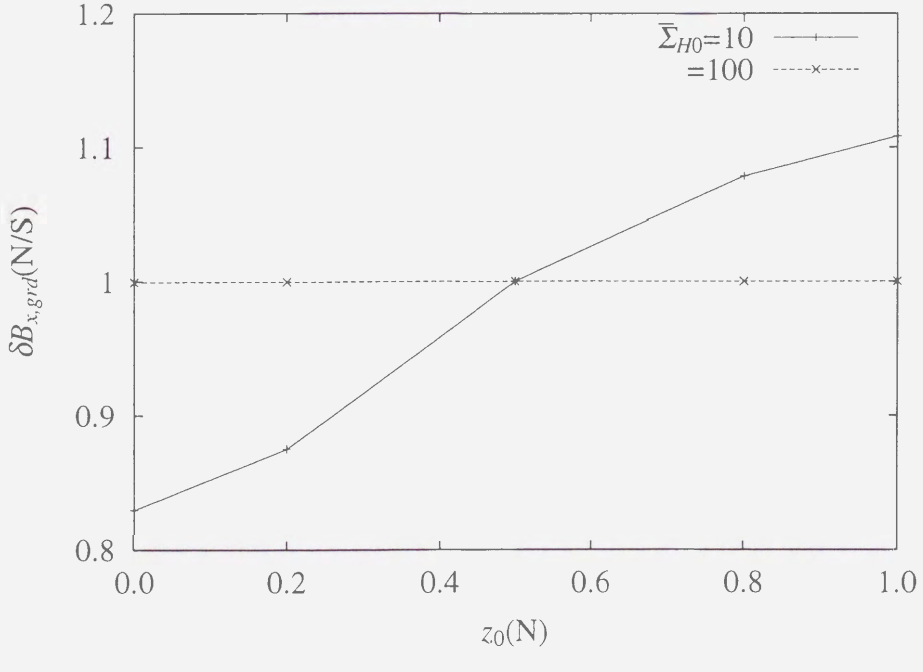

Figure 3.8: $\delta B_{x,grd}$(N/S) as a function of z_0(N). z_0(S) = 0 and $\bar{\Sigma}_{P0}$(N,S) = 10. $\bar{\Sigma}_{H0}$(N,S) is 10 (solid line) and 100 (dashed line).

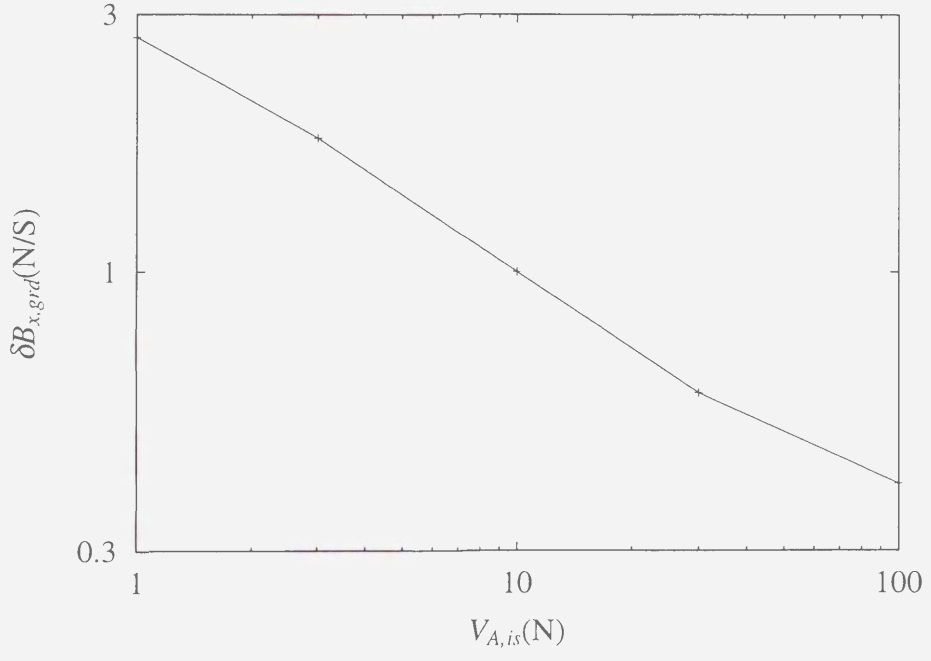

Figure 3.9: $\delta B_{x,grd}$(N/S) as a function of $V_{A,is}$(N). $V_{A,is}$(S) = 10, z_0(N,S) = 0 and $\bar{\Sigma}_{P0}$(N,S) = $\bar{\Sigma}_{H0}$(N,S) = 10.

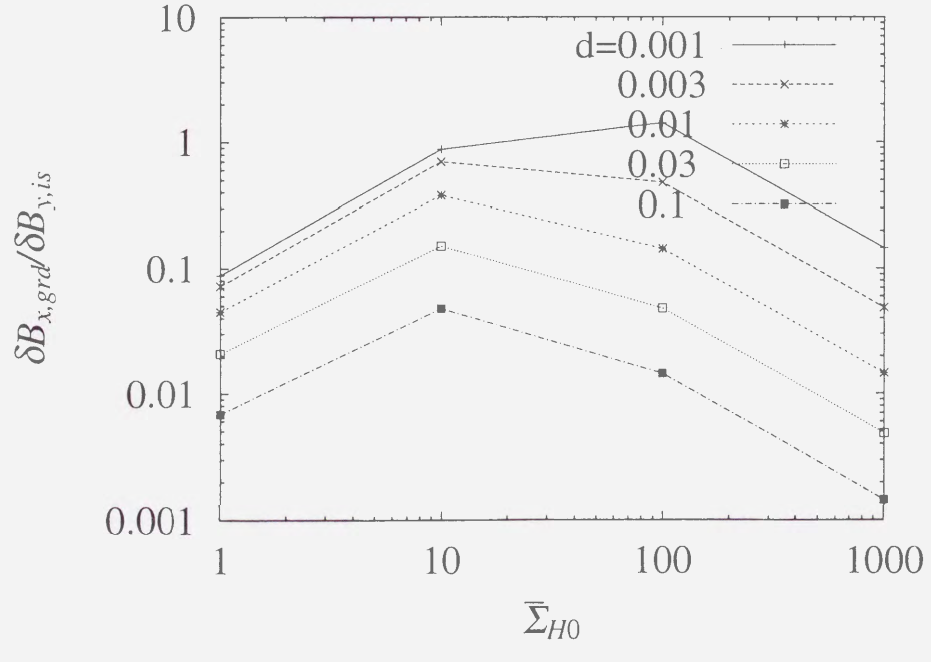

Figure 3.10: $\delta B_{x,grd}/B_{y,is}$ as a function of Hall conductivity for various values of d (0.001, 0.003, 0.01, 0.03, 0.1).

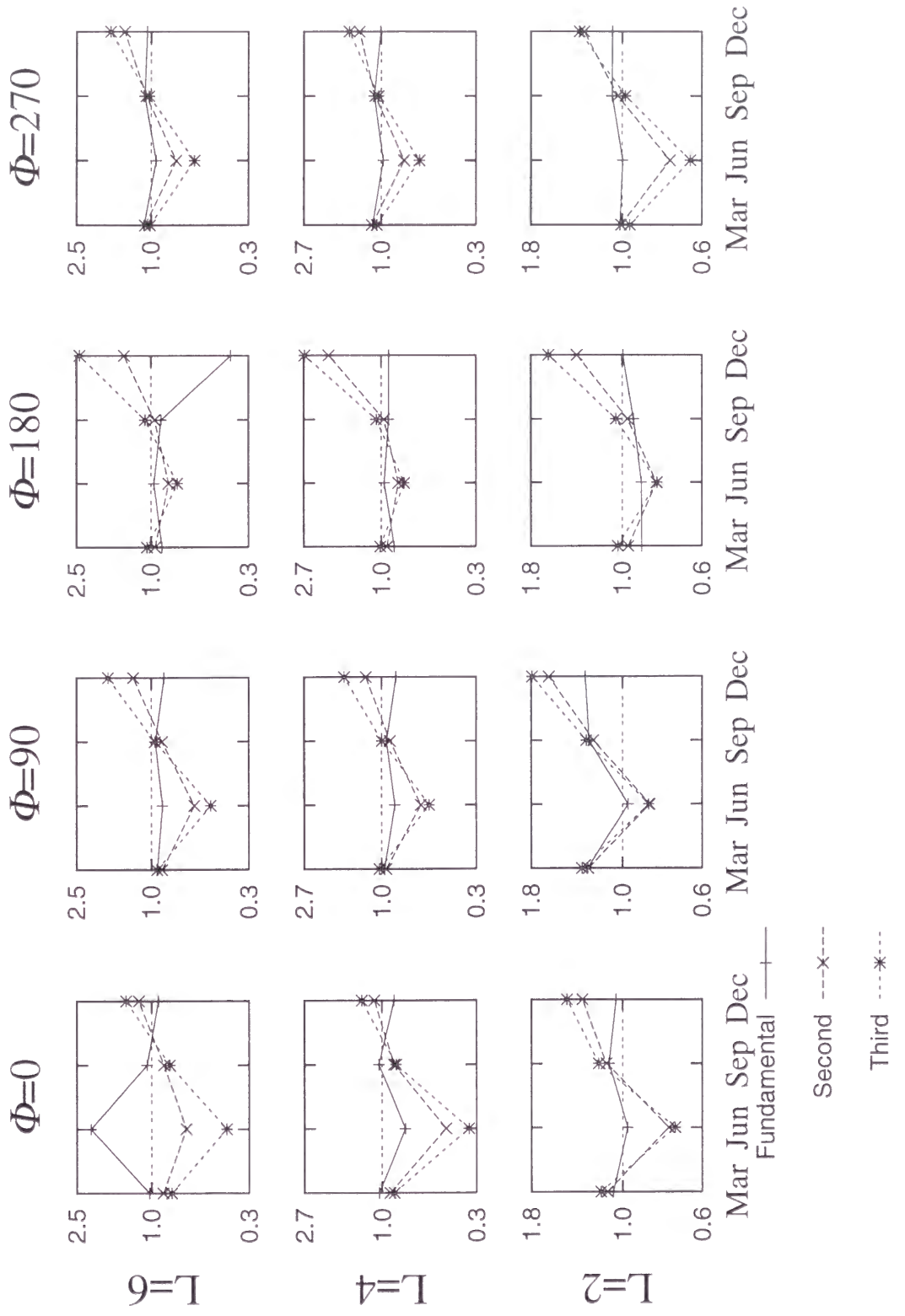

Figure 4.1: $\delta B_{x,grd}$(N/S) calculated with realistic parameters. The top, middle and bottom panel are L=6, 4 and 2. Each column shows Magnetic Longitude =0°, 90°, 180° and 270° from left to right. The solid, dashed and dotted lines show the fundamental, second and third harmonics respectively.

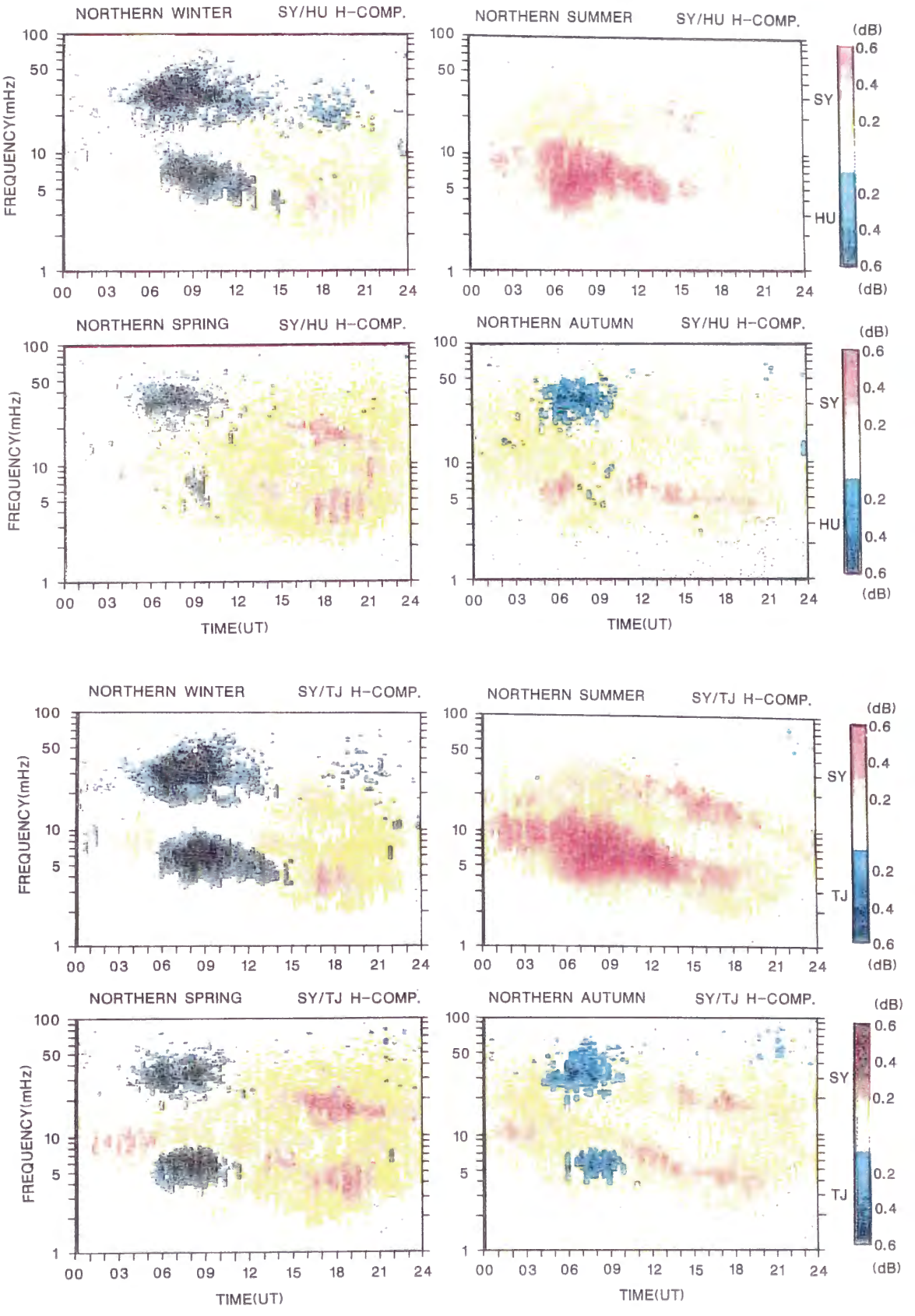

Figure 4.2: North-South asymmetries of Pc 3-5 pulsations in Syowa-Iceland conjugate pairs. [Saito *et al.*, 1989] (Top) The power ratio of the pulsations in Syowa-Husafell conjugate pair. (Bottom) That of Syowa-Tjörnes pair.

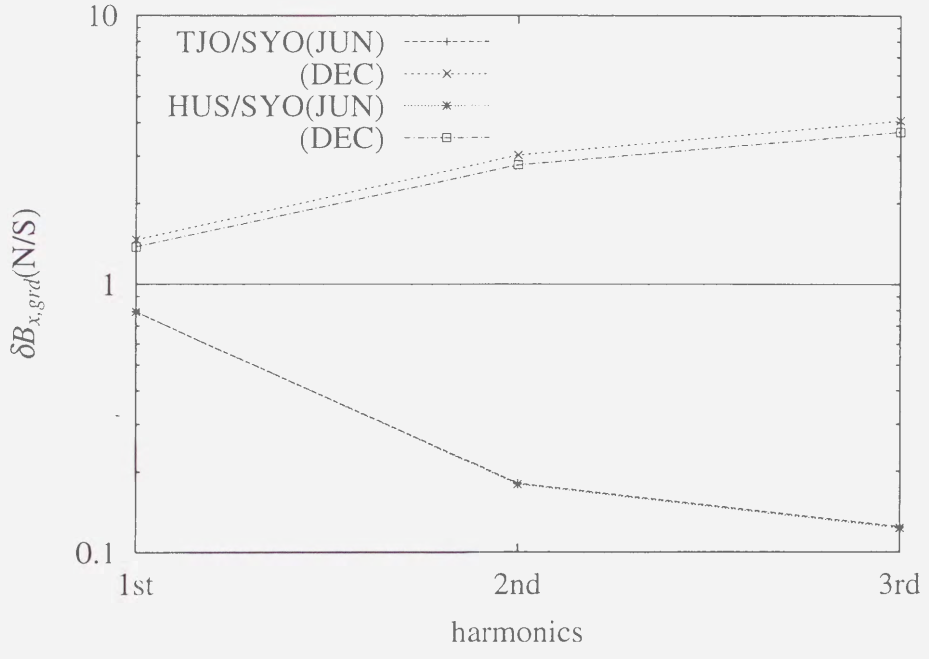

Figure 4.3: The north-south ratio of the Syowa-Iceland conjugate pairs calculated with the parameter estimated from IGRF95 and IRI90.

This thesis is based on the following paper.

Ground magnetic perturbations associated with the standing toroidal mode oscillations in the magnetosphere-ionosphere system,
submitted to Earth, Planets and Space,
by H. Nakata, S. Fujita, A. Yoshikawa, M. Itonaga and K. Yumoto

Acknowledgements

The author wishes to express his grateful thanks to Dr. S. Fujita for his advise and supports throughout this study. The author also sincerely wishes to thank Prof. T. Araki for encouragements, valuable discussions and giving the chance to tackle this study. Special thanks are also due to Drs. A. Yoshikawa and M. Itonaga for helpful discussions. Prof. K. Yumoto encourages the author and kindly offered the author the result on the north-south asymmetries of the ground magnetic perturbations observed in the 210° MM observation. The author is indebted to Dr. M. Takeda for his help of calculating the ionospheric conductivity. The author is also grateful to Drs. S. Machida, T. Iyemori, T. Kamei, A. Saito and other colleagues of Kyoto University for helpful comments and discussions. Numerical calculations were performed by the Computer Center of the National Institute of Polar Research.